Mineralium Deposita (2020) 55:1535–1560
https://doi.org/10.1007/s00126-019-00934-z

ARTICLE

Parental magma, magmatic stratigraphy, and reef-type PGE enrichment of the 2.44-Ga mafic-ultramafic Näränkävaara layered intrusion, Northern Finland

Ville Järvinen[1] · Tapio Halkoaho[2] · Jukka Konnunaho[3] · Jussi S. Heinonen[1] · O. Tapani Rämö[1]

Received: 28 February 2019 / Accepted: 6 November 2019 / Published online: 31 December 2019

Abstract

About 20 mafic-ultramafic layered intrusions in the northern Fennoscandian shield were emplaced during a widespread magmatic event at 2.5–2.4 Ga. The intrusions host orthomagmatic Ni-Cu-PGE and Cr-V-Ti-Fe deposits. We update the magmatic stratigraphy of the 2.44-Ga Näränkävaara mafic-ultramafic body, northeastern Finland, on the basis of new drill core and outcrop observations. The Näränkävaara body consists of an extensive basal dunite (1700 m thick), and a layered series comprising a peridotitic–pyroxenitic ultramafic zone (600 m thick) and a gabbronoritic–dioritic mafic zone (700 m thick). Two reversals are found in the layered series. The composition of the layered series parental magma was approximated using a previously unidentified marginal series gabbronorite. The parental magma was siliceous high-Mg basalt with high MgO, Ni, and Cr, but also high SiO_2 and Zr, which suggests primary magma contamination by felsic crust. Cu/Pd ratio below that of primitive mantle implies PGE-fertility. The structural position of the marginal series indicates that the thick basal dunite represents an older wallrock for the layered intrusion. A subeconomic reef-type PGE-enriched zone is found in the border zone between the ultramafic and mafic zones and has an average thickness of 25 m with 150–250 ppb of Pt + Pd + Au. Offset-type metal distribution and high sulfide tenor (50–300 ppm Pd) and R-factor (10^5) suggest reef formation by sulfide saturation induced by fractional crystallization. The reef-forming process was probably interrupted by influx of magma related to the first reversal. Metal ratios suggest that this replenishing magma was PGE-depleted before emplacement.

Keywords Näränkävaara · Finland · Layered intrusion · Magmatic stratigraphy · Parental magma · PGE reef

Introduction

The Paleoproterozoic mafic-ultramafic Näränkävaara layered intrusion, northern Finland, is the easternmost member of the Tornio-Näränkävaara layered intrusion belt, which comprises six mafic-ultramafic layered intrusions with an average age of 2440 Ma (Fig. 1) (Alapieti 1982; Iljina & Hanski 2005). The intrusions were emplaced during widespread mantle-driven igneous activity related to extension and rifting of the Archean nucleus of the Fennoscandian shield (Amelin & Semenov 1996; Tiira et al. 2014; Huhma et al. 2018). In total, approximately 20 early Paleoproterozoic layered intrusions with associated dyke swarms have been found in the NW region of the Fennoscandian shield (Finland, Russia, and Sweden), all with ages between 2.53–2.39 Ga (Alapieti et al. 1990; Amelin et al. 1995; Vuollo & Huhma 2005; Bayanova et al. 2009).

The intrusions at the Archean-Proterozoic boundary in northern Finland have significant exploration potential for orthomagmatic mineral deposits, and have been shown to host reef-, contact-, and offset-type PGE(±Ni-Cu) deposits and Cr-Fe-Ti-V deposits (Huhtelin 2015; Iljina et al. 2015; Karinen et al. 2015; Makkonen et al. 2017). Mafic-ultramafic layered intrusions elsewhere with similar structure and composition as

Editorial handling: F. Molnar

Electronic supplementary material The online version of this article (https://doi.org/10.1007/s00126-019-00934-z) contains supplementary material, which is available to authorized users.

✉ Ville Järvinen
ville.jarvinen@helsinki.fi

[1] Department of Geosciences and Geography, University of Helsinki, Gustaf Hällströmin katu 2 (Physicum), P.O. Box 64, 00014 Helsinki, Finland

[2] Geological Survey of Finland, Neulaniementie 5, P.O. Box 1237, 70211 Kuopio, Finland

[3] Geological Survey of Finland, Lähteentie 2, P.O. Box 77, 96101 Rovaniemi, Finland

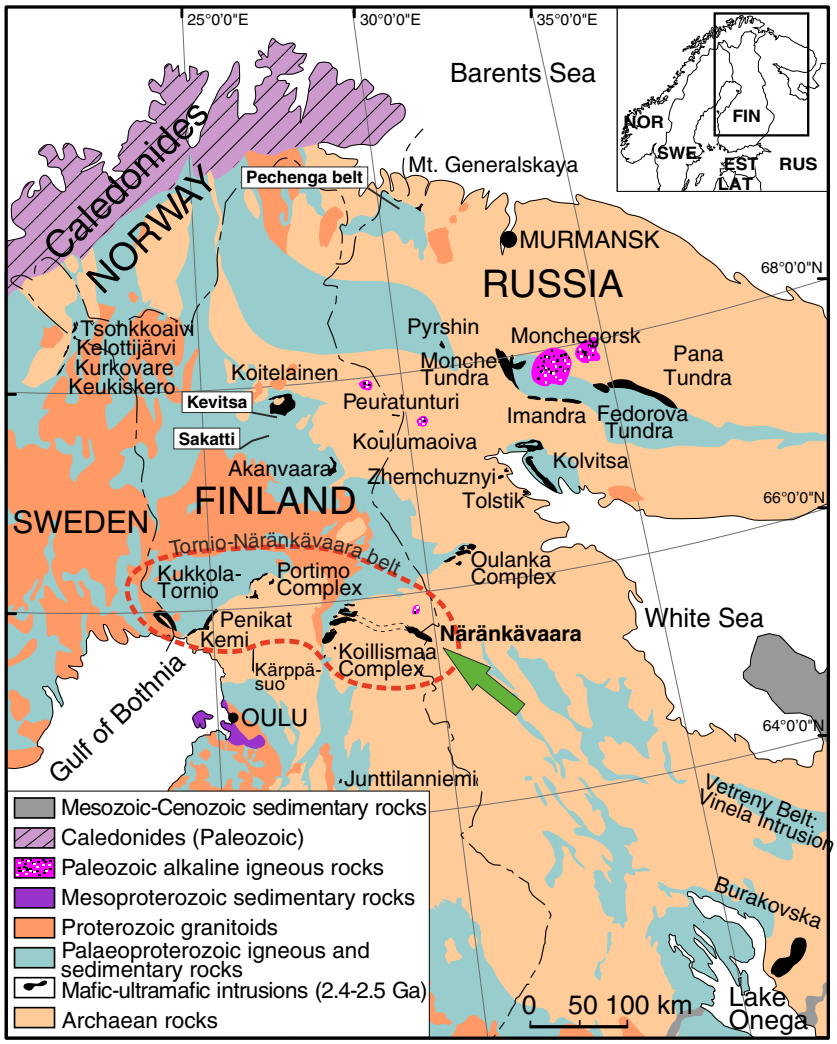

Fig. 1 Map of the 2.53–2.39 Ga mafic-ultramafic layered intrusions of the Fennoscandian shield. The 2.44-Ga Tornio-Näränkävaara belt of layered intrusions outlined in red (Iljina & Hanski 2005), with study area pointed out with an arrow. The Koillismaa complex includes the tectonically dismembered Western Intrusions and Näränkävaara to the east, connected by a positive magnetic and gravity anomaly presumed to be a "hidden dyke" (dashed line, see Fig. 2) (Alapieti 1982). Modified after Alapieti et al. (1990)

the Näränkävaara intrusion, e.g., the Great Dyke of Zimbabwe (Wilson 1996) and the Munni Munni complex in Western Australia (Hoatson & Keays 1989), also host high-grade PGE reefs.

Geological mapping and exploration projects have been conducted in the Näränkävaara intrusion since the 1950s (Auranen 1969; Piirainen et al. 1978; Alapieti 1982; Iljina 2003; Vesanto 2003; Lahtinen 2005; Akkerman 2008; Halkoaho et al. 2019). The recent discovery of a ~ 2-km-thick homogeneous unit of dunite along the southern contact of the Näränkävaara layered series highlights the need to re-evaluate the structure, composition, and exploration potential of the Näränkävaara body (Lahtinen 2005; Halkoaho et al. 2017, 2019).

In this study, we refine the magmatic stratigraphy of the Näränkävaara mafic-ultramafic body, originally presented by Alapieti (1982). We also discuss the parental magma composition of the intrusion as inferred from the newly found marginal series gabbronorite. We also describe a new uneconomic sulfide-associated stratiform (reef-type) PGE-enriched zone, located in the contact between the ultramafic and mafic zones of the Näränkävaara layered series, and present a model that explains the low grade of the PGE mineralization.

Geological background

Tornio-Näränkävaara layered intrusion belt

The intrusions of the Tornio-Näränkävaara belt (Fig. 1) are typical mafic-ultramafic layered intrusions with marginal and layered magmatic series (Alapieti & Lahtinen 2002). The intrusions were emplaced within Archean granitoids along the rifting craton margin, and are now located along the contact between the Archean granite-gneiss basement and Karelian Paleoproterozoic supracrustal rocks (Iljina & Hanski 2005). The zircon U-Pb ages of the intrusions range between 2.45 and 2.43 Ga (Alapieti 1982; Huhma et al. 1990;

Iljina 1994; Mutanen & Huhma 2001; Perttunen & Vaasjoki 2001; Maier et al. 2018).

The layered intrusions of the Fennoscandian shield have been classified into three compositional types: (1) mafic-ultramafic (e.g., Kemi, Näränkävaara), (2) mafic (Akanvaara, Koitelainen, Koillismaa), and (3) megacyclic (Portimo, Penikat) (Alapieti & Lahtinen 2002). The parental magmas have been thought to be (boninite-like) siliceous high-Mg basalts (SHMB), usually classified into high-Cr and low-Cr types (Alapieti et al. 1990; Iljina & Hanski 2005). The high-Cr and low-Cr magma types may be related by fractional crystallization (Maier et al. 2018). Whole-rock and isotope geochemical results (average ε_{Nd} of −2) point to crustal contamination of primary magmas from mantle plume sources (Puchtel et al. 1997; Hanski et al. 2001; Vuollo & Huhma 2005; Yang et al. 2016; Maier et al. 2018).

Näränkävaara mafic-ultramafic body

The Näränkävaara intrusion was emplaced into the Taivalkoski block of the Western Karelian subprovince of the Fennoscandian shield. Unlike other intrusions of the Tornio-Näränkävaara belt, Näränkävaara is surrounded on all sides by Archean (~2.8 Ga) granitoids (Fig. 2) (Hölttä et al. 2012). The N-S trending 2.9–2.8 Ga Suomussalmi greenstone belt terminates about 10 km south of the Näränkävaara body (Fig. 2) (Lehtonen et al. 2017), and the recently discovered (likely Archean) Takanen greenstone belt also borders the body 2 km to the NW (Iljina 2003). The large SW-NE trending Oulujärvi shear zone crosscuts the NW side of Näränkävaara.

Historically, the Näränkävaara layered intrusion has been included as part of the Koillismaa Layered Intrusion Complex (KLIC) (Alapieti 1982). The KLIC comprises (1) the tectonically dismembered western intrusion blocks, (2) the eastern Näränkävaara intrusion, and (3) a strong positive gravity and magnetic anomaly that connects the first two (Fig. 1 and inset in Fig. 2). Alapieti (1982) interpreted the Koillismaa and Näränkävaara intrusions to be co-genetic, with the Näränkävaara intrusion representing the lowest stratigraphic level of the complex. The connecting geophysical anomaly was interpreted as a magmatic conduit that fed the two intrusions.

Based on geophysical observations, the Näränkävaara mafic-ultramafic body is about 30 km long and 5 km wide and extends to a depth of 5–10 km with steep outer contacts (Elo 1992; Salmirinne & Iljina 2003). It has been considered to represent a 2436 ± 5 Ma mafic-ultramafic layered series, composed of a peridotitic-pyroxenitic ultramafic zone, and a gabbroic-dioritic mafic zone (Fig. 2) (Alapieti 1982). Later studies have shown that the Näränkävaara body includes two other distinct ultramafic cumulate units (Iljina 2003; Lahtinen 2005). Firstly, an extensive, up to 2 km thick basal dunite, composed of homogeneous olivine meso- and adcumulate, borders the layered series along its southern contact. In recent drilling, the dunite was also discovered on the northern side of the layered series and so may partly envelop it (Fig. 2; Akkerman 2008). Secondly, a series of smaller elongate intrusions, composed of harzburgite with coarse poikilitic orthopyroxene, are found crosscutting the basement complex parallel to the northern contact of the layered series ("northern ultramafics" in Fig. 2). These two cumulate units have only been described in mineral exploration reports (Iljina 2003; Vesanto 2003; Lahtinen 2005; Akkerman 2008; Halkoaho et al. 2019) and a thesis (Telenvuo 2017), and their petrogenetic relationship to the layered series remains to be determined.

The strike of the igneous layering in the pyroxenites of the Näränkävaara layered series is generally parallel to the long axis of the intrusion (Fig. 3a). A large SW-NE fault separates the intrusion into two main blocks, with the NW block dipping about 15–25° to the NE, and the SE block dipping 5–20° to the SW (Fig. 2) (Alapieti et al. 1979). Complex block faulting is present throughout the intrusion with several smaller strike-slip faults that have strikes along the short axis of the intrusion and dip-slip faults that have strikes along the long axis. The layered series is mostly undeformed and unaltered by post-magmatic processes, whereas the basal dunite is thoroughly serpentinized.

Materials and methods

A large part of the materials in this study were compiled from previously unpublished results of exploration projects conducted by the Geological Survey of Finland (GTK) and private exploration companies in 1966–2008 (Auranen 1969; Iljina 2003; Akkerman 2008). Most important results originate from 22 drill holes (named in Fig. 2) drilled or revisited by Outokumpu Mining Oy in 2001–2003 (Vesanto 2003; Lahtinen 2005). These form a profile across the NW block of the Näränkävaara body. New drilling was conducted in the SE block of the Näränkävaara body by the GTK in 2017–2018 (Halkoaho et al. 2019), and one drill hole intersecting a marginal series melagabbronorite is included in this study (R1 in Fig. 2). Five representative outcrop samples collected during this time are also included. Drill logs can be found in Appendix 1.

Whole-rock compositions were determined by X-ray fluorescence (XRF) from pressed powder pellets at Labtium Oy laboratories (method code 175/176X), and at the University of Oulu, Finland. Some base metals and trace elements were determined by inductively coupled plasma optical emission spectrometry (ICP-OES) following Aqua Regia digestion (Labtium Oy, method code 510P). The REE were determined

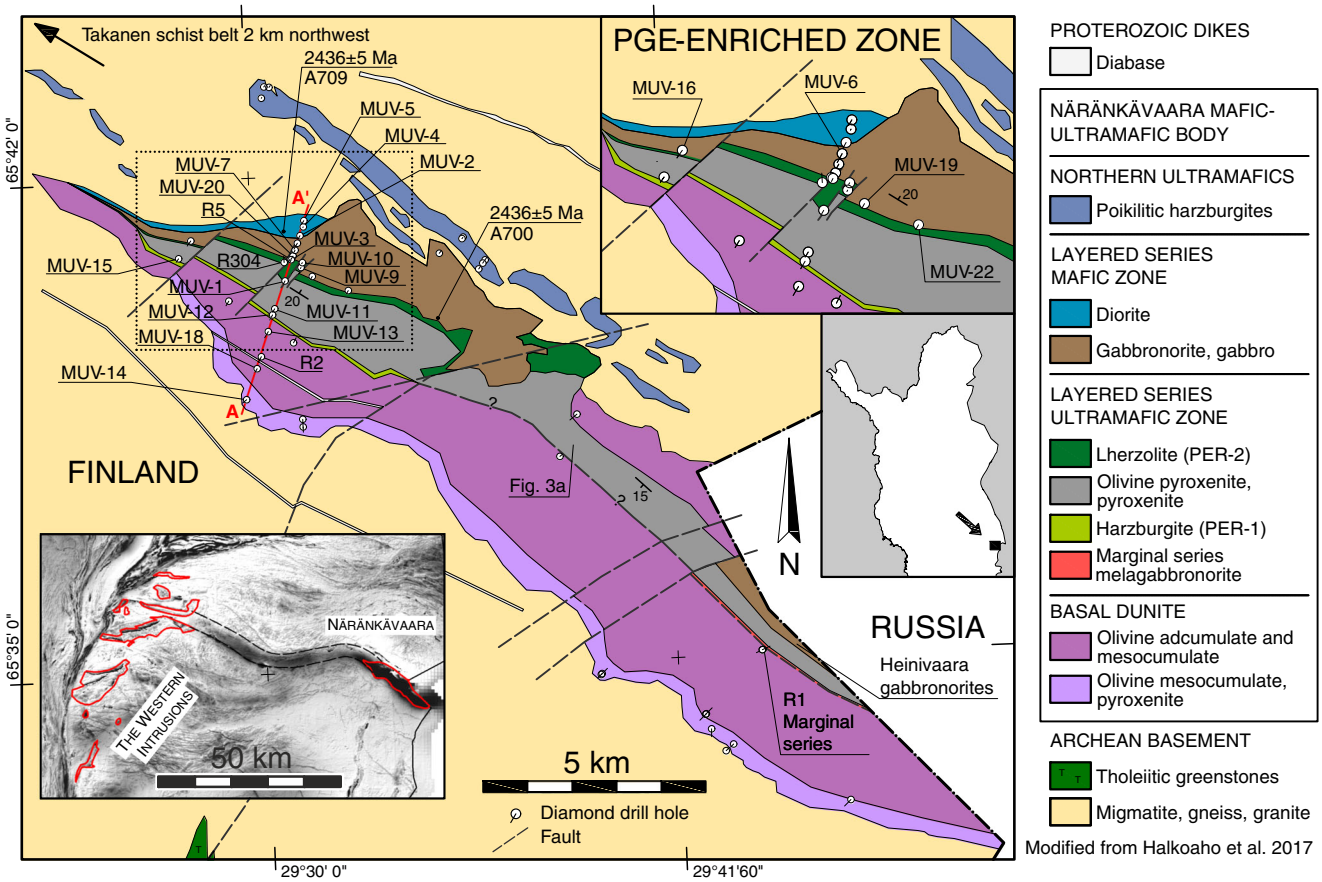

Fig. 2 Geological map of the Näränkävaara mafic-ultramafic body. Line A–A' marks cross-section in Fig. 4. Drill holes labeled in the top right inset intersect the reef-type PGE-enriched zone (SL reef). Inset on bottom left shows Näränkävaara and the Western Intrusion blocks of the Koillismaa complex outlined in red over a total magnetic intensity map (connecting magnetic anomaly outlined with a dashed line, see text). Marginal series melagabbronorite was only intersected in drill-hole R1

by inductively coupled plasma mass spectrometry (ICP-MS) following HF–$HClO_4$ digestion and lithium metaborate–sodium perborate fusion (Labtium Oy, method code 308 M); some trace elements were analyzed by ICP-OES after the same digestion and fusion procedure (Labtium Oy, method code 308P). Precious metals (Pt, Pd, Au) were determined

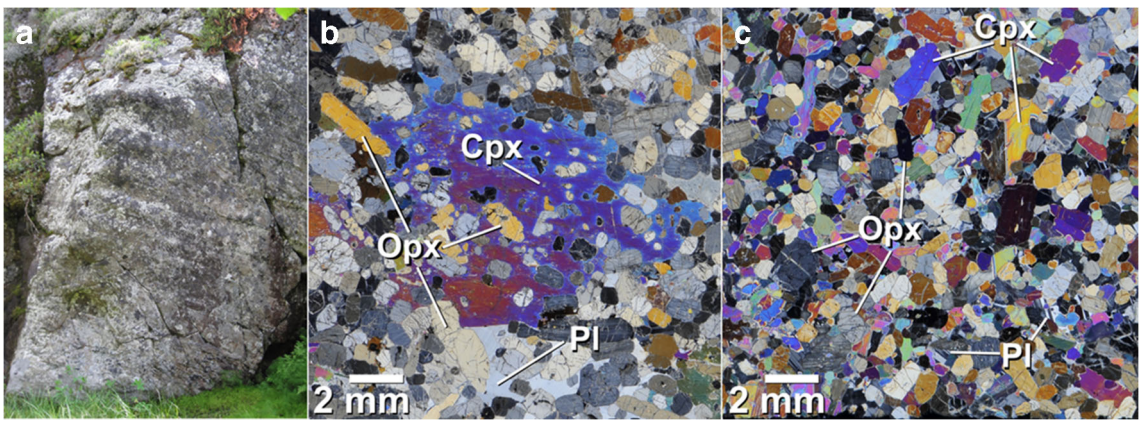

Fig. 3 **a** Rhythmic ~30-cm-thick igneous layers in an unaltered pyroxenite of unit PX-1 near the top of the Näränkävaara hill (photo location indicated in Fig. 2; a vertical outcrop with a height of 4 m). **b** Plagioclase-websterite of unit PX-2 with sparse but coarse poikilitic augite (sample *MUV-19 38.75m*). This typically barren rock type forms the foot-wall for the PGE-enriched zone. Thin section image, crossed polarizers. **c** Plagioclase-websterite of unit PX-2 with ~50% fine-medium-grained augite (sample *MUV-22 12.87m*). Typical host rock of the reef-type PGE-enriched zone (SL reef). Thin section image, crossed polarizers. All photos by V. Järvinen

by graphite furnace atomic absorption spectroscopy (GFAAS) or by ICP-OES following Pb-fire assay fusion at Labtium Oy (method code 705 U/P); with some analyses (Pt, Pd, Au, Ru, Rh, Ir, Os) made by ICP-MS following NiS-fire assay fusion at Labtium Oy (method code 714 M) or at Intertek Laboratories (method code NS25/MS), Australia. Major oxides were normalized to volatile-free 100%. All iron is presented as FeO^{tot}. Whole-rock analyses comprise 1242 XRF, 1519 Au + Pd + Pt (2PGE + Au) and 22 REE analyses. All analytical data and detailed descriptions of methods and detection limits (Labtium Oy 2015) can be found in Appendix 2.

Mineral chemistry was determined for four thin sections from the PGE-enriched zone using wavelength dispersive spectroscopy of a Cameca SX100 electron microprobe at the Finnish Geosciences Research Laboratory in Espoo, with a total of 129 analyses from 58 mineral grains (Appendix 2). Mineral abbreviations used according to Whitney & Evans (2010).

Revised magmatic stratigraphy of the NW block of the Näränkävaara body

A new cross section across the NW block the Näränkävaara mafic-ultramafic body was constructed based on compilation and interpretation of historical drill core logs, new thin section studies, and correlation of whole-rock compositions between drill hole intersections (Fig. 4). A new stratigraphic column based on this cross section is presented in Fig. 5. The stratigraphy consists of a 1700 m thick basal dunite (purple in Fig. 5); and a layered series consisting of a 600-m-thick ultramafic zone (gray) and a 700-m-thick mafic zone (brown), with two compositional reversals found in the layered series (green).

Drill hole spacing leads to stratigraphic gaps of up to 500–600 m in the basal dunite, but the layered series is intersected completely up to a quartz-dioritic unit at the top. The contact between the layered series and the basement complex on the northern side of the body is not intersected. A large oblique fault causes the southern side of the cross section to be uplifted 300 m in relation to the northern side, allowing a stratigraphic section of about 1300 m of the layered series to be observed (Fig. 4).

Lithology and petrography

Basal dunite

In general, the basal dunite is composed of fine- to medium-grained olivine adcumulate and lesser olivine mesocumulate with coarse poikilitic orthopyroxene. Chromite is found in trace amounts in both cumulus and intercumulus (poikilitic) habits. The dunite is completely serpentinized but pseudomorphs after olivine and pyroxenes commonly exhibit undeformed cumulate textures and conventional igneous classification terminology for the rocks can thus be used. Proterozoic diabase dykes up to 100 m thick cut the unit.

The basal dunite has been divided into three units based on lithology and whole-rock composition. The first unit consists of dunite and harzburgite (BD-1 in Figs. 4 and 5, 250–500 m thick). The unit forms a marginal or transition zone against the basement complex, with olivine adcumulate grading into harzburgites towards the basement contact. The harzburgites nearest to contact also contain trace amounts of clinopyroxene, plagioclase and phlogopite. The unit BD-1 contains the single olivine analysis made from the basal dunite formation with composition $Fo_{87.5}$ (Alapieti 1982). The basement contact is tectonized with the basal dunite truncating foliation in the foot wall. Near to the contact, the unit contains xenoliths of Archean basement rocks.

The second, volumetrically largest dunite unit (BD-2 in Figs. 4 and 5, 1000–1500 m thick) is composed of massive olivine adcumulates with minor mesocumulate interlayers. This unit contains poikilitic chromite, which is typically only described from komatiites (Barnes & Hill 1995).

The third unit (BD-3 in Figs. 4 and 5, 50–100 m thick) consists of olivine adcumulates with patches of olivine mesocumulates with up to 20 vol% coarse poikilitic pyroxene. The contact of the basal dunite (unit BD-3) and the basal peridotite of the layered series (unit PER-1) is intersected by two drill holes (Fig. 4). Still, the exact location and nature of the contact is ambiguous due to strong alteration and decomposition of the basal dunite and the lowermost section of the basal peridotite. There is an approximately 50-m-thick and strongly altered contact zone, where the basal dunite transitions into harzburgite as the amount of orthopyroxene increases from 5–10 vol% to 40–60 vol%, coinciding with fining of orthopyroxene grain size from coarse poikilitic to granular. Grain boundaries between olivine and orthopyroxene are commonly embayed. After the transition zone, the degree of serpentinization decreases, with the cumulates of the overlying layered series being relatively unaltered.

Marginal series gabbronorite

In the SE block of the Näränkävaara body, a marginal series gabbronorite was found in the contact of the basal dunite and the layered series, on the side of the layered series (drill hole R1 in Fig. 2). Contact of the basal dunite and the layered series is sharp, tectonized, and subvertical, with surface magnetometry indicating a lateral extent of 5–6 km. The basal dunite near the contact consists of serpentinized olivine

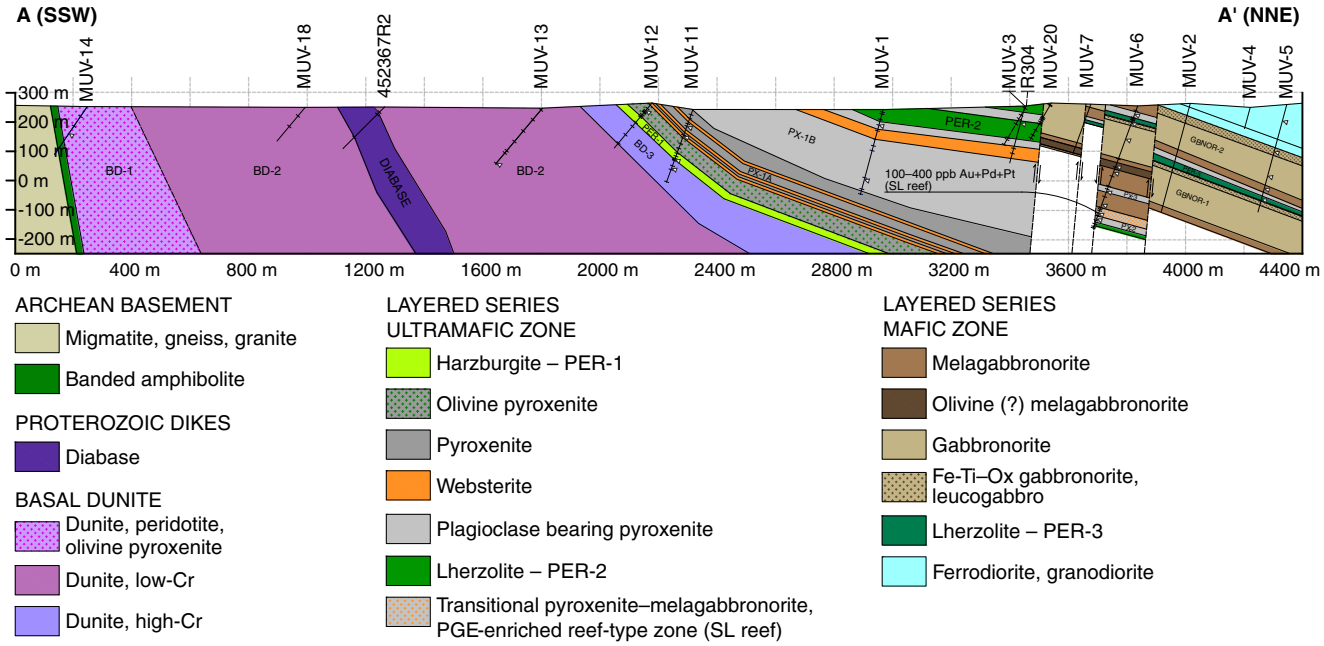

Fig. 4 Cross section of the NW block of Näränkävaara (A–A' in Fig. 2), with the PGE-enriched zone (SL reef) pointed out. Marginal series melagabbronorite has not been found along this cross section (cf. Figure 2). For stratigraphic position of labeled units see Fig. 5. Drill hole traces in black lines: perpendicular thin lines mark thin section locations; arrows mark whole-rock analyses in Table 1. Interpreted faults in dashed lines. MUV-1 thin section descriptions from Telenvuo (2017), others from this study

mesocumulates with 10–20 vol% coarse poikilitic pyroxene. The marginal series is about 10 m thick and composed of non-cumulus textured melagabbronorite with up to 5 vol% biotite and < 1 vol% chalcopyrite and pyrrhotite. The marginal series grades into the pyroxenites of the layered series over a distance of 1–2 m. Marginal series has not been found from the NW block of the intrusion (that is, in Figs. 4 or 5).

Ultramafic zone of the layered series

Along the NW cross section the contact between the basal dunite and the ultramafic zone of the layered series dips about 45 ° to the NNE (Fig. 4). The peridotitic-to-pyroxenitic ultramafic zone is about 600 m thick (~ 1750–2350 m in Fig. 5). The cumulates are generally well preserved and exhibit magmatic layering with a dip of 15–20° NNE (Fig. 3a).

Above the transitional contact zone with the basal dunite, the layered series begins with harzburgitic to olivine pyroxenitic unit (PER-1 at height ~ 1750 m in Fig. 5). The unit consists of olivine-bronzite adcumulates with up to 60 vol% olivine. Disseminated chromite is found in trace amounts throughout the ultramafic zone of the layered series (Alapieti 1982; Telenvuo 2017). The rocks gradate from harzburgite to olivine bronzitite within a distance of 50 m. The last 20 m of the olivine-pyroxenite contains up to 3 vol% pyrrhotite-dominated interstitial sulfides (note S in Fig. 5) (Telenvuo 2017).

The following 120-m-thick pyroxenitic unit PX-1A is composed of bronzitite and websterite (Fig. 4; note CaO-rich websterite interlayers in Fig. 5). The lower half of the unit contains massive and almost monomineralic bronzitites with minor intercumulus augite and trace plagioclase. In the upper half of the unit, rhythmic interlayers of websterite appear, composed of coarse grained bronzite-augite adcumulates, some with trace olivine. The overlying 250-m-thick pyroxenitic unit, PX-1B, is composed of rhythmic (plagioclase)-websterites; these are bronzite-mesocumulates with 5–20 vol% poikilitic augite and 1–5 vol% intercumulus plagioclase. The amount of plagioclase increases upwards in stratigraphy. About 70 m before the next unit (the PER-2 reversal) there is a 20-m-thick bronzite-augite adcumulate interlayer, after which the amount of intercumulus plagioclase again increases to 5–10 vol%. This last plagioclase-websteritic subunit hosts a PGE-enriched intersection with up to 200 ppb of Pd + Pt + Au (2PGE + Au; see Fig. 5 at height ~ 2150 m) similar to the main PGE-enriched zone hosted in the unit PX-2 after the PER-2 reversal.

The reappearance and rapid increase in the amount of cumulus olivine at a stratigraphic height of 2200 m marks the beginning of the unit PER-2, which is the first of the two lithological reversals within the layered series. The unit is about 120 m thick, and includes two roughly 50 m thick subunits composed of lherzolites and olivine pyroxenites separated by a olivine free pyroxenitic interlayer similar in composition to unit PX-1B. The lherzolites are composed of olivine-bronzite ortho- and mesocumulates with up to 60 vol% olivine, coarse (up to 1–2 cm in diameter) poikilitic augite, and up to 10 vol% intercumulus plagioclase. Chromite and

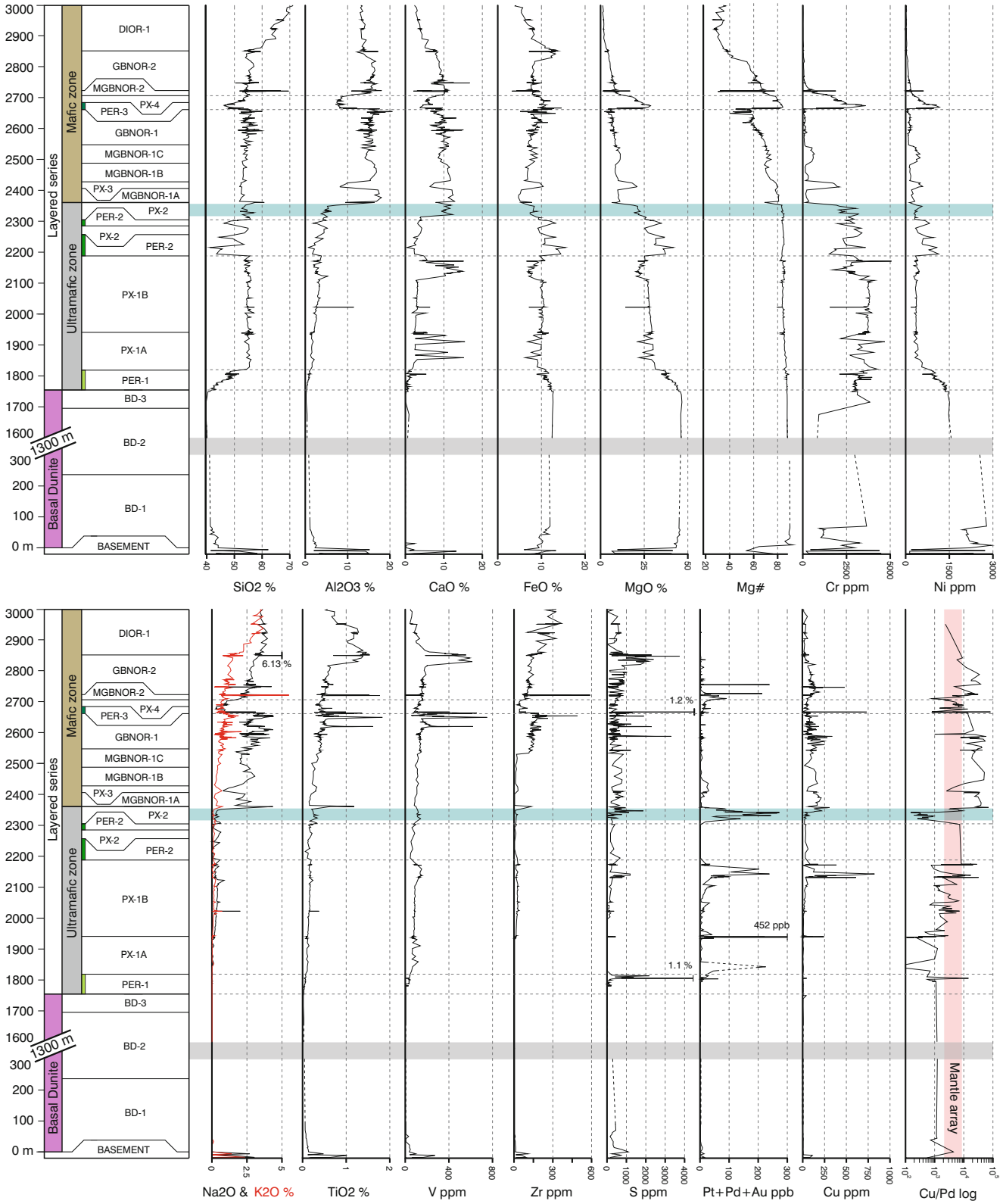

Fig. 5 Magmatic stratigraphic column of the NW block of the Näränkävaara mafic-ultramafic body with whole rock compositional variations. There is a 1300-m gap in the basal dunite due to lack of drilling and analyses (highlighted with gray). The reef-type PGE-enriched zone (SL reef) is highlighted in blue, peridotitic units outlined with dashed lines

phlogopite appear in trace amounts. The unit is generally sulfide-poor with occasional grains of trace pyrrhotite, but intersections with up to 1 vol% of disseminated pyrrhotite with minor pentlandite and chalcopyrite are found in drill hole R5 (Fig. 2).

The ultramafic zone ends with the 50–60 m thick pyroxenitic unit PX-2, composed of rhythmic websteritic mesocumulates, similar to those in unit PX-1B. Augite is typically found as relatively scarce and coarse oikocrysts (Fig. 3b). Over the last 20–30 m, the amount of augite and intercumulus plagioclase increases (Fig. 3c) and the cumulates grade into melagabbronorites of the mafic zone. This last gradational subunit of the ultramafic zone contains < 0.5 vol% of disseminated sulfides, and hosts a reef-type PGE-enriched zone that will be described in detail later (highlighted in Fig. 5).

Mafic zone of the layered series

The gabbronoritic-to-dioritic mafic zone is about 700 m thick (~ 2350–3000 m in Fig. 5). The zone is defined by the appearance of cumulus plagioclase, which increases upwards from 20 to 50 vol% in the melagabbronorites and pyroxenites to 50–70 vol% in the gabbronorites (note Al_2O_3 in Fig. 5). The plagioclase-dominated gabbroic cumulates of the mafic zone are generally more massive and have less well developed magmatic layering compared to the cumulates of the ultramafic zone.

In the first 200 m of the mafic zone, plagioclase alternates between cumulus and intercumulus. The first unit of this melagabbronoritic subzone (MGBNOR-1A) is a 40-m-thick melagabbronorite composed of plagioclase-augite-bronzite adcumulate. It is followed by a 20-m-thick pyroxenitic unit (PX-3, note Cr and Ni in Fig. 5) composed of augite-bronzite mesocumulate with 5–25 vol% intercumulus plagioclase. The subzone ends with two 60-m-thick melagabbronoritic units composed of augite-bronzite mesocumulates with 30–50 vol% intercumulus plagioclase (MGBNOR-1B and -1C), with the latter unit richer in bronzite making it relatively Ni- and Cr-rich (Fig. 5; labeled as olivine melagabbronorite in Fig. 4). First disseminated ilmenite grains appear in the last few meters of unit MGBNOR-1C. All four units contain up to 1 vol% of fine grained disseminated intercumulus pyrrhotite, chalcopyrite and pentlandite.

Increase in cumulus plagioclase to > 50 vol% and decrease in the amount of pyroxene marks the beginning of the 120-m-thick gabbronoritic unit GBNOR-1 at the stratigraphic height of ~ 2550 m (note increase in Zr in Fig. 5). Plagioclase is found as a cumulus phase until the last lithologic reversal (unit PER-3), and the lower half of the unit is composed of homogeneous plagioclase-augite-broznite cumulates. Disseminated magnetite appears 50 m from the base of the unit increasing upwards in stratigraphy. Minor amounts of interstitial biotite, as well as up to 1 vol% of trace sulfides, are found throughout this unit. From halfway up the unit heterogeneity increases with the occurrence of 0.20- to 2-m-thick leucopegmatoidal (anorthositic) layers and sparse coarse-grained plagioclase-quartz-(calcite) veining; quartz and localized coarse-grained sulfides and oxides are variably associated with the pegmatoidal layers. Biotite increases upwards in stratigraphy (note K_2O in Fig. 5), appearing as evenly distributed 2–5 mm clumps, equigranular to plagioclase and pyroxenes; based on texture it is interpreted as magmatic (i.e., not potassic alteration). The gabbronorites end in a 20-m-thick Fe-Ti-oxide-rich gabbronorite with up to 10 vol% biotite and leucopegmatoidal interlayers.

The second and last compositional reversal is at the stratigraphic height of ~ 2650 m (unit PER-3 in Figs. 4 and 5). The lower contact is a 1-m-thick pegmatoidal melagabbro with up to 5 vol% coarse pyrrhotite and chalcopyrite (see S in Fig. 5). The contact is followed by the 30- to 40-m-thick unit PER-3 comprising olivine-pyroxenitic and minor lherzolitic ortho- and mesocumulates containing up to 30–40 vol% olivine. The unit is strongly altered (serpentinized) and disequilibrium textures are common, with, e.g., pyroxene exsolution, embayed and intergrown grain boundaries, and secondary tremolite-rims found on augite grains. The unit is also distinctly phlogopite-rich (5–15 vol%) with poikilitic phlogopite enclosing pyroxenes and olivine. The amount of olivine decreases upwards as cumulates grade into the last pyroxenitic unit PX-4. This unit is relatively altered, consisting of bronzite-augite ortho- and mesocumulate with up to 20 vol% intercumulus phlogopite and trace plagioclase.

As plagioclase increases upwards, the rocks are first melagabbronorites of the unit MGBNOR-2, and then, with plagioclase again becoming a cumulus mineral, the last 130-m-thick gabbronorites of the layered series (unit GBNOR-2 in Figs. 4 and 5). These follow roughly the same trend as the previous gabbronoritic unit, with irregular gabbropegmatoidal layers, trace amounts of disseminated sulfides, and appearance of disseminated ilmenite soon followed by magnetite. The gabbronorites grade into a light colored quartz dioritic unit composed first of ferrodiorite and then granodiorite (Figs. 4 and 5).

Whole-rock compositional variations

Type samples reflecting the calculated average whole-rock compositions of the units comprising the basal dunite and the layered series are presented in Table 1. Variations in whole-rock compositions are illustrated in Figs. 5, 6, and 7.

Table 1 Whole-rock compositions of type samples from the Näränkävaara mafic-ultramafic body. Samples selected to reflect calculated average unit compositions. Sample locations marked with arrows in Fig. 4

Unit	BD-1	BD-2	BD-3	PER-1	PX-1A	PX-1A	PX-1A	PX-1B	PX-1B	PER-2	PX-2	PX-2
drill hole	MUV-14	MUV-13	MUV-11	MUV-11	MUV-12	MUV-11	MUV-11	MUV-12	MUV-1	MUV-3	MUV-6	MUV-6
depth (m)	111.40	244.00	215.00	184.60	31.00	60.00	97.00	46.00	76.30	62.00	410.60	391.00
rock type	*Dun*	*Dun*	*Dun*	*Hzb*	*Ol-Pyx*	*Brz*	*Wb*	*Pl-Brz*	*Pl-Wb*	*Lhz*	*Pl-Brz*	*Pl-Wb*
wt%												
SiO_2	44.11	39.74	41.81	44.27	52.38	55.24	54.38	54.48	54.06	45.19	54.47	52.05
TiO_2	0.14	0.01	0.03	0.04	0.10	0.10	0.13	0.14	0.20	0.13	0.25	0.26
Al_2O_3	2.31	0.11	0.35	0.53	1.47	1.50	1.46	2.67	3.13	2.50	4.51	6.16
FeO	9.46	12.62	12.26	11.87	10.12	9.89	6.27	10.37	8.35	12.79	9.75	9.00
MnO	0.11	0.19	0.20	0.19	0.24	0.22	0.17	0.24	0.21	0.21	0.20	0.17
MgO	43.23	47.06	44.42	42.47	33.67	30.09	21.96	28.59	21.75	36.58	26.09	22.67
CaO	0.30	0.13	0.56	0.27	1.64	2.58	15.20	2.76	11.44	2.17	3.83	9.44
Na_2O	< 0.03	< 0.03	< 0.03	< 0.03	< 0.03	< 0.03	0.09	0.28	0.39	< 0.03	0.43	0.20
K_2O	0.01	< 0.003	< 0.003	< 0.003	0.02	0.02	0.02	0.08	0.24	0.13	0.16	0.04
P_2O_5	0.02	< 0.006	< 0.006	< 0.006	< 0.006	< 0.006	< 0.006	< 0.006	< 0.006	0.02	0.02	< 0.006
ppm												
Ba	22	< 20	< 20	21	23	20	27	22	109	54	56	< 20
Cl	354	2375	3068	2483	393	< 100	< 100	< 100	534	876	< 100	100
Cr	2962	1173	3131	3056	3432	3401	3045	3720	2044	2556	2688	2410
Cu	< 20	< 20	< 20	< 20	< 20	< 20	< 20	< 20	208	30	20	50
Ni	2215	1513	1366	1280	765	421	319	356	385	956	386	390
Rb	< 10	< 10	< 10	< 10	< 10	< 10	< 10	< 10	14	< 10	< 10	< 10
S	1096	< 100	< 100	< 100	107	< 100	< 100	< 100	259	< 100	287	300
Sc	< 20	< 20	< 20	< 20	< 20	< 20	56	< 20	43	< 20	< 20	30
Sr	< 10	< 10	< 10	< 10	< 10	< 10	16	28	80	42	51	20
V	37	< 10	< 10	< 10	48	65	119	82	145	56	100	110
Zn	84	89	66	72	64	74	39	78	71	79	72	60
Zr	11	< 10	< 10	< 10	< 10	< 10	< 10	20	31	22	16	20
ppb												
Au	< 2	< 2	< 2	< 2	< 2	< 2	< 2	< 2	81	< 2	< 2	2
Pd	< 2	< 3	< 2	< 2	35	< 2	< 2	4	28	< 3	11	205
Pt	< 2	< 2	< 2	< 2	13	< 2	< 2	3	26	< 2	8	37

Abbreviations for rock types: *Dun* = Dunite; *Hzb* = Harzburgite; *Ol-Pyx* = Olivine-pyroxenite; *Brz* = Bronzitite; *Pl-Brz* = Plagioclase-bronzitite; *Pl-Wb* = Plagioclase-websterite; *Lhz* = Lherzolite. Elements Au, Pd, and Pt analyzed by GFAAS, other elements by XRF.

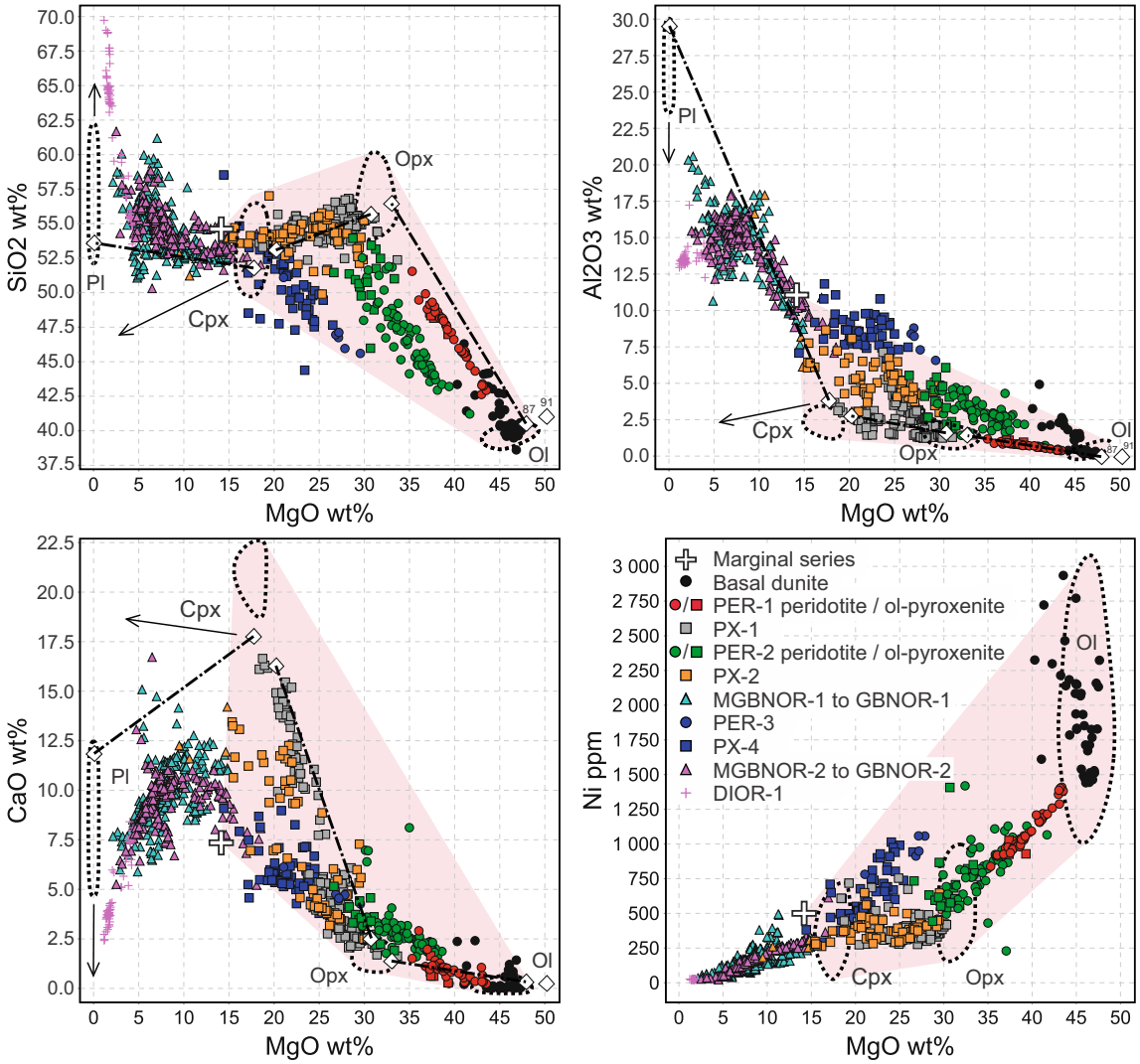

Fig. 6 Whole-rock SiO_2, Al_2O_3, CaO, and Ni plotted against MgO for the Näränkävaara layered series and basal dunite. Unit names in legend correlate to units in Fig. 5. Fields in dashed lines indicate measured mineral compositions of olivine (Ol), orthopyroxene (Opx), clinopyroxene (Cpx), and plagioclase (Pl) (Alapieti 1982; Telenvuo 2017). White diamonds show respective mineral compositions from MELTS model results (Ol, Opx, Cpx, Pl; see text); tie-lines (dash-dot) connect mineral compositions at steps where the crystallizing phase changes or a new phase begins to crystallize; arrow indicates how the mineral composition changes after beginning of plagioclase fractionation; numbers indicate olivine Fo content. Shaded area connects the marginal series composition to Ol-Opx-Cpx composition fields, illustrating that the chemistry of the ultramafic cumulates can roughly be explained as mixtures of these components

Basal dunite

In general, the serpentinized basal dunite is geochemically homogeneous and poor in most elements except Ni and Cr. On average, the Mg#[1] is 88, with normalized MgO between 40 and 47.5 wt% and SiO_2 between 39 and 43 wt%. Exception is the unit BD-1, that contains a transitional zone with increasing SiO_2, TiO_2, Al_2O_3, V, and Zr towards the basement contact (e.g., up to 5 wt% Al_2O_3 with 41 wt% MgO; see Fig. 5). Unit BD-2 is the most MgO-rich with 45–47.5 wt% MgO; and it also has a lower Cr contents of 1000–1500 ppm, compared to the other two dunite units with 2000–4000 ppm Cr. Ni varies between 1600 and 2900 ppm in units BD-1 and BD-2, decreasing to less than 1500 ppm in unit BD-3. Variable Ni content at constant MgO (see Fig. 6) implies extraction of Ni-sulfides, but the basal dunite samples along the NW profile are very sulfide poor. PGEs in the basal dunite are typically below the detection limit of 2 ppb (66 out of 74 samples) with the highest assay being 15 ppb Pt + Pd. High Cl concentrations of 1000–4500 ppm are present

[1] Formula used for calculation of Mg#: $100 \times ((X_{MgO}/40.3044)/((X_{MgO}/40.3044) + (0.9 \times (X_{FeO}^{tot}/71.8464))))$; where X is wt% oxide.

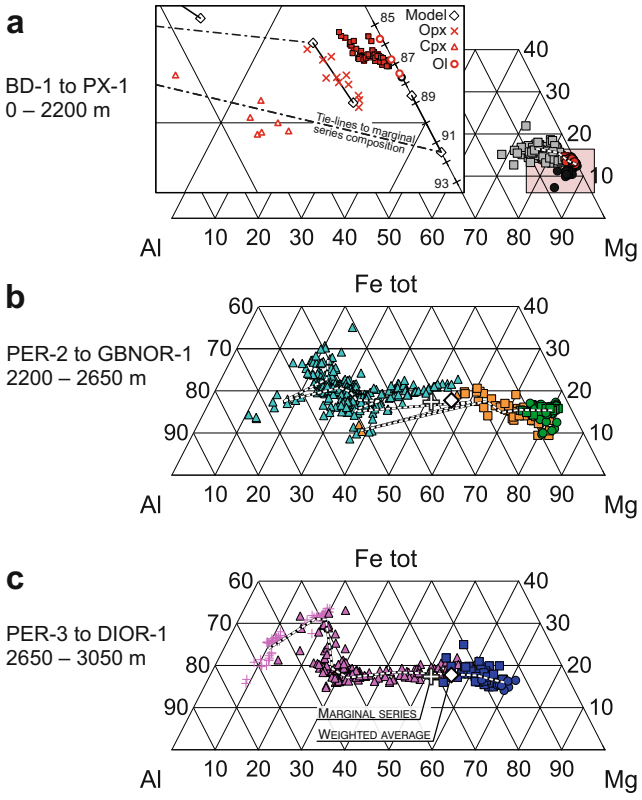

Fig. 7 Whole-rock compositions of the Näränkävaara basal dunite and layered series cumulates on Mg-Fe-Al plots, divided into three plots according to the two compositional reversals in the layered series (units PER-2 and PER-3 in Fig. 5). See Fig. 6 for legend. Also plotted are the whole-rock composition of the marginal series gabbronorite, and the layered series weighted average (labeled). Continuous tie-lines (black-white dash) connect average unit compositions in stratigraphic order. **a** Stratigraphic sequence from BD-1 to PX-1. Shaded area in *inset* showing whole-rock compositions of units PER-1 and PX-1A; measured (unfilled red symbols) and modeled (white diamonds; see text) mineral compositions, with numbers indicating olivine Fo contents. Extrapolating the cumulate compositions to the Mg-Fe axis indicates an average of ~$Fo_{87.5}$ **b** Stratigraphic sequence from PER-2 to GBNOR-1, note small-scale reversals related to the transition from the ultramafic to mafic zone (units MGBNOR-1A to 1C, see Fig. 5). **c** Stratigraphic sequence from PER-3 to DIOR-1

throughout the basal dunite. Moving from the basal dunite into the layered series there is an approximately 4–5 wt% decrease in MgO and 5–6 wt% increase in SiO_2.

Marginal series gabbronorite

The composition of the marginal series gabbronorite intersected in drill hole R1 is presented in Table 2 and plotted in Figs. 6 and 7. The composition is characterized by high SiO_2 (54–55 wt%) relative to MgO (14–15 wt%) (Fig. 6), and low CaO (6.5–7.5 wt%) and TiO_2 (0.4 wt%); Ni (300–500 ppm) and Cr (1450–1750 ppm) are also relatively high. The Mg# is 77, Al/Ti ratio is 20, and Ca/Al ratio 0.7. According to IUGS classification, the composition is boninitic, with $SiO_2 >$ 52 wt%, MgO > wt.8%, and $TiO_2 < 0.5$ wt% (Le Bas 2000); and according to the Jensen cation diagram the composition is of a komatiitic basalt (Jensen 1976).

Layered series

The general magmatic evolution of the layered series is reflected in variations of MgO and Mg# with height (Fig. 5). There is a stepwise descent from the ultramafic to the mafic zone through the melagabbronoritic transition zone, followed by a gradual decrease into the dioritic unit. This trend is interrupted by the two peridotitic reversals. Compositions continue to become more evolved after each reversal, and cumulate sequences after each successive peridotite plot on a similar (tholeiitic) fractionation trend as seen in the Mg-Fe-Al plots in Fig. 7a–c.

Variations in whole-rock compositions correlate well with changes in mineral abundances determined by thin section petrography. The ultramafic zone is characterized mainly by the accumulation of orthopyroxene and clinopyroxene, and also olivine associated with the peridotitic units PER-1 and PER-2. Clinopyroxene contains up to 0.5–1 wt% Cr_2O_3, and orthopyroxene about half of this. Olivine usually contains > 2000 ppm Ni, with the highest measured Ni-contents of 3128 ppm (Alapieti 1982; Telenvuo 2017). This leads to high MgO, Cr, and Ni concentrations in the ultramafic zone (Fig. 5, Table 1). The websteritic interlayers are geochemically distinct, with up to 17 wt% CaO (Figs. 5 and 6). Increase in modal intercumulus clinopyroxene and plagioclase causes a steady increase of CaO and Al_2O_3 towards the mafic zone (Fig. 5), with the last plagioclase-pyroxenites of unit PX-1B containing up to 4.4 wt% Al_2O_3.

Zirconium concentrations correlate with observed cumulate textures. In the ultramafic zone, the primitive adcumulate pyroxenites of unit PX-1A contain < 10 ppm Zr, that increases to 20–40 ppm in the mesocumulatic pyroxenite and melagabbronorite units above (Fig. 5). Zirconium concentrations stay around this level, until increasing sharply to 100–250 ppm at the

Table 2 Whole-rock compositions of potential Näränkävaara layered series parental magmas (marginal series, weighted average), with comparisons from Finnish 2.45 Ga dykes and the Koillismaa complex, Bushveld, and the Vetreny Belt

Sample	Näränkävaara marginal series gabbronorite[a]	Näränkävaara marginal series gabbronorite[b]	Näränkävaara weighted average	Average Finnish 2.45 Ga boninite-norite dyke[c]	Koillismaa complex chilled margin[d]	High-MgO basalt, Vetreny Belt[e]	Bushveld B1[f]
wt%							
SiO_2	54.94	54.29	55.37	53.38	53.69	51.38	55.74
TiO_2	0.27	0.52	0.48	0.63	0.28	0.64	0.34
Al_2O_3	10.70	11.34	9.66	12.32	16.64	11.53	11.82
FeO	7.75	9.42	9.07	10.07	7.11	10.72	9.45
MnO	0.14	0.16	0.17	0.16	0.13	0.18	0.18
MgO	14.47	13.79	15.89	11.30	9.18	14.16	11.85
CaO	7.48	7.2	6.41	8.06	9.84	9.42	6.50
Na_2O	3.38	2.33	1.83	2.24	2.56	1.37	1.63
K_2O	0.85	0.84	0.89	0.63	0.52	0.53	0.98
P_2O_5	0.02	0.11	0.09	0.09	0.02	0.09	0.08
ppm							
Ba	180	300	304	204	291	158	364
Cl	8200	2300	264	*n.a.*	841	*n.a.*	*n.a.*
Cr	1680	1820	1441	962	464	1309	965
Cu	30	70	62	67	125	*n.a.*	51
Ni	480	530	298	308	218	391	284
S	300	600	247	144	52	*n.a.*	396
Sr	600	210	229	179	367	160	198
Zn	50	80	70	80	60	*n.a.*	90
La	6.1	12.2	*n.a.*	9.1	6.6	8.7	18.0
Ce	13.0	24.4	*n.a.*	18.4	11.4	17.8	34.8
Pr	1.5	2.8	*n.a.*	1.8	1.3	*n.a.*	4.2
Nd	5.7	11.7	*n.a.*	8.8	4.8	9.9	15.5
Sm	1.1	2.4	*n.a.*	2.0	0.8	2.3	2.8
Eu	0.4	0.7	*n.a.*	0.7	0.5	0.7	0.8
Gd	1.2	2.4	*n.a.*	1.7	0.9	2.4	2.4
Tb	0.2	0.4	*n.a.*	0.3	0.1	*n.a.*	0.3
Dy	1.1	2.3	*n.a.*	1.7	0.7	2.6	1.9
Ho	0.2	0.5	*n.a.*	0.3	0.2	*n.a.*	0.4
Er	0.7	1.4	*n.a.*	1.0	0.5	1.6	1.1
Tm	0.1	0.2	*n.a.*	0.2	*b.d.l.*	*n.a.*	0.2
Yb	0.7	1.4	*n.a.*	1.2	0.5	1.6	1.1
Lu	0.1	0.2	*n.a.*	0.2	*b.d.l.*	*n.a.*	0.2
Hf	1.6	1.6	*n.a.*	1.7	*n.a.*	1.6	1.9
Y	6.1	11.8	12	14.0	5.1	13.5	11.7
Nb	< 3	< 3	*n.a.*	2.3	*n.a.*	4.7	4.2
Ta	< 1	< 1	*n.a.*	0.2	*n.a.*	0.1	0.5
Rb	34	30	32	23	11	13	40
Th	4.2	3.4	*n.a.*	2.0	0.7	1.4	3.5
U	1.2	0.8	*n.a.*	0.4	*n.d.*	0.3	l1.0
Zr	44	60	88	69	24	59	77
Sc	23	24	14	*n.a.*	24	34	30
V	165	150	136	189	102	185	239
Co	58	58	*n.a.*	44	*n.a.*	63	59

Table 2 (continued)

Sample	Näränkävaara marginal series gabbronorite[a]	Näränkävaara marginal series gabbronorite[b]	Näränkävaara weighted average	Average Finnish 2.45 Ga boninite-norite dyke[c]	Koillismaa complex chilled margin[d]	High-MgO basalt, Vetreny Belt[e]	Bushveld B1[f]
ppb							
Au	1.2	2.4	*n.a.*	0.88	*b.d.l.*	*n.a.*	2.72
Pd	5.5	6.7	*n.a.*	6.17	*b.d.l.*	*n.a.*	13.99
Pt	7.8	8.6	*n.a.*	7.11	*b.d.l.*	*n.a.*	19.36

[a] This study (drill hole R1 170.70 m); [b] this study (drill hole R1 173.70 m); [c] Maier et al. 2001; [d] Karinen 2010 (Porttivaara block, sample 259-TKK-00); [e] Puchtel et al. 1997 (Sample 3901); [f] Barnes et al. 2010. Näränkävaara marginal series elements from SiO2 to Zn analyzed with XRF; from La to U with ICP-MS; from Zr to Co with ICP-OES; and from Au to Pt with GFAAS. Näränkävaara weighted average calculated from XRF analyses.

n.a. not analyzed, *b.d.l.* below detection limit

beginning of the first homogeneous gabbronorite unit GBNOR-1. This indicates a change in crystallization into strongly orthocumulate or even liquid compositions, with a higher fraction of trapped Zr-enriched residual melt present in the rocks. Increasing K_2O contents towards the top of unit GBNOR-1 appears to be associated with increase in modal biotite.

Whole-rock compositional differences between units PER-1 and PER-2 are relatively small compared to PER-3. Average MgO content decreases from 41 wt% in PER-1, to 33 wt% in PER-2, and to 24 wt% in PER-3 (Fig. 6 and Table 1). Concentrations of incompatible elements are similarly much higher in PER-3 (e.g., Al_2O_3 in Fig. 6). In relation to the low MgO contents, PER-3 contains high Ni (average 850 ppm) and Cr (average 3000 ppm), similar to the other two peridotitic units (Fig. 6). These characteristics correlate with available olivine analyses: average olivine in PER-1 is Fo_{87} with 2000 ppm Ni; in PER-2 it is Fo_{84} with 1800 ppm Ni (Alapieti 1982; Telenvuo 2017); and in PER-3 it is Fo_{82} with 3000 ppm Ni (from author, unpublished data).

The transition from the ultramafic to mafic zone of the layered series comprises a 200 m interval from the top of unit PX-2 to the bottom of unit GBNOR-1. This melagabbronorite subzone includes several smaller reversals in which compositions of, e.g., CaO, FeO^{tot}, MgO, Al_2O_3, Ni, and Cr oscillate by up to 10% (Figs. 5 and 7b). The compositional fluctuations get smaller with height and decreasing Mg#, ceasing at the beginning of the relatively homogeneous gabbronorite unit GBNOR-1. The most distinct lithological change in this transition zone is plagioclase becoming a cumulus phase, which causes a sharp rise in Al_2O_3, from 7.5 wt% in unit PX-2 to 15–17 wt% in MGBNOR-1A.

In the ultramafic zone, two relatively S-rich zones with 200–1300 ppm S are found approximately 50 m above and below the unit PER-2. The zone above PER-2 hosts a continuous reef-type PGE-enriched zone (highlighted in Fig. 5), described in detail below. Both zones are enriched in PGEs with 100–500 ppb of 2PGE + Au, with the zone below PER-2 also containing slightly elevated Cu contents of 500–1100 ppm.

Trace disseminated Fe-Cu sulfides are common in the mafic zone, with S concentrations fluctuating around 500 ppm (Fig. 5). The first gabbronorite (GBNOR-1) marks the beginning of Fe-Ti-oxide accumulation. Two minor oxide related peaks in Fe-Ti-V concentrations are found, both with < 700 ppm V. The second peak is found in the gabbronorite-diorite contact, and is associated with disseminated oxides and sulfides. This contact zone contains on average 1700 ppm S but no appreciable PGE (~ 2850 m in Fig. 5), and probably signifies terminal sulfide saturation caused by increasing SiO_2 and decreasing FeO^{tot} concentrations.

REE and other lithophile elements

The chrondrite-normalized (CN) REE pattern (Fig. 8a and Table 2) of the marginal series gabbronorite is LREE enriched, with a gentler slope after Sm. La_{CN}/Yb_{CN} is 5.7, La_{CN}/Sm_{CN} is 3.2, and Gd_{CN}/Yb_{CN} is 1.3, with a slight negative Eu-anomaly (Eu/Eu* = 0.85–1). The trace element pattern (Fig. 8b) is strongly fractionated relative to primitive mantle (PM). The mobile large ion lithophile elements (LILE; Rb, Ba, Sr), and Th and U, are enriched 40–60 times relative to PM (e.g., 200–600 ppm Sr). Both Nb and Ta are below detection limits (Nb < 3 ppm or $Nb_{PM} < 4.5$; Ta < 1 ppm or $Ta_{PM} < 25$). The immobile

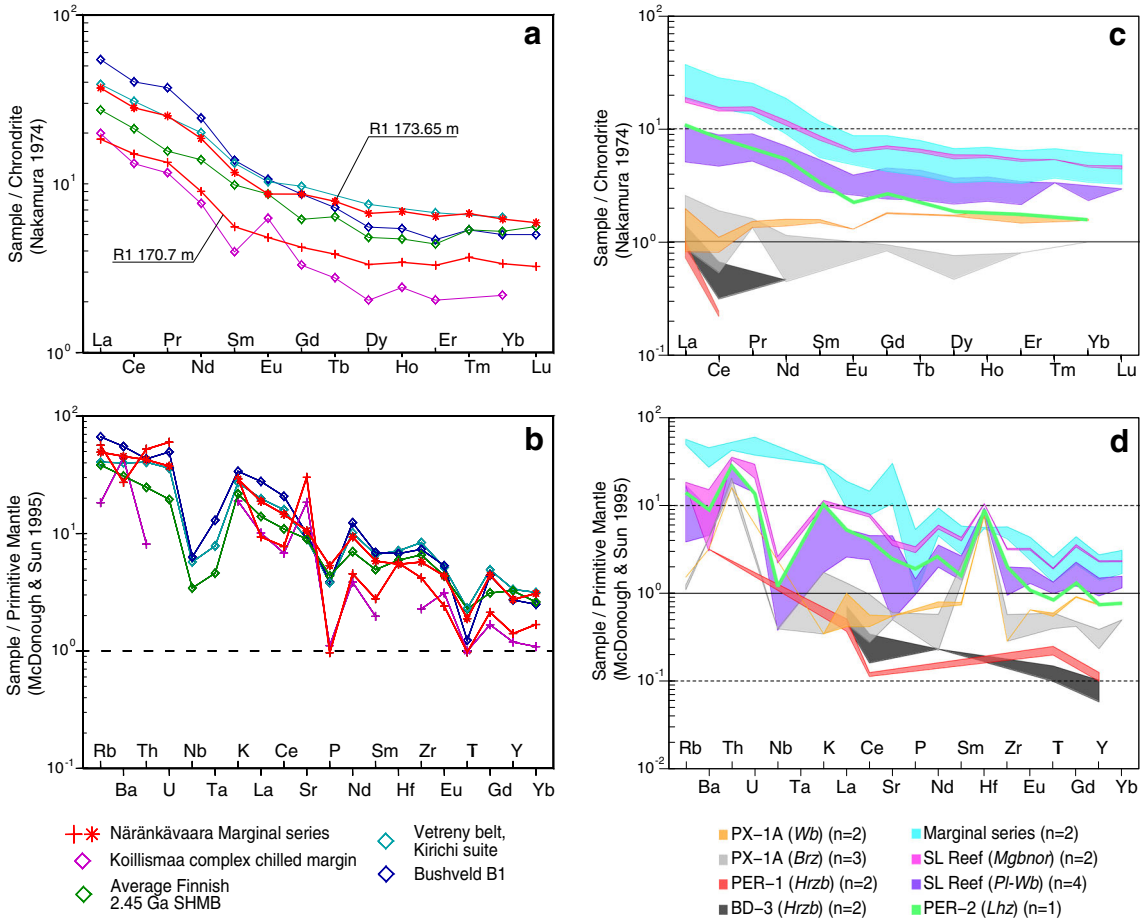

Fig. 8 **a** Chondrite-normalized (Nakamura 1974) REE-patterns; and **b** Primitive mantle-normalized (McDonough & Sun 1995) trace element patterns of the marginal series gabbronorite of the Näränkävaara marginal series melagabbronorite (red), with comparisons to other 2.45 Ga Fennoscandian SHMB and komatiitic basalts (Puchtel et al. 1997; Barnes et al. 2010; Karinen 2010; Maier et al. 2018) **c** Grouped chondrite-normalized REE-patterns and **d** grouped primitive mantle-normalized trace-element patterns of whole-rock cumulate samples from the Näränkävaara basal dunite and the layered series. Unit names correlate with Fig. 5. *Hrzb* harburgite, *Lhz* lherzolite, *Brz* bronzitite, *Wb* websterite, *Pl-Wb* plagioclase-bearing websterite, *Mgbnor* melagabbronorite

and less incompatible high field strength elements from La onward have concentrations 2–10 times those of PM with a gently falling slope that is interrupted by negative Ti and P anomalies.

Whole-rock samples from units BD-3, PER-1, PX-1A, PER-2, PX-2, and MGBNOR-1 have been analyzed for REE (Fig. 8c, Table 2). REE values in all cumulate units are below those of the marginal series gabbronorite. Analyses from units BD-3 and PER-1 are generally below detection limits. REE values in bronzitites and websterites of unit PX-1A are close to chondritic, with flat or weakly LREE-enriched patterns. REE concentrations and LREE-enrichment increase from PER-2 upwards, with units PER-2 and PX-2 containing La_{CN} of ~ 10 on average. Total REE values correlate with whole-rock Zr, suggesting that the REE values of the ultramafic cumulates mainly indicate the relative amount of trapped intercumulus melt.

Characteristics of trace element patterns of cumulate samples (Fig. 8d) are similar to the marginal series gabbronorite, showing enrichment in Th and U, and depletion in Nb, Ta, Ti, and P. The cumulates are Hf-rich with 2–3 ppm Hf (~ 10 times PM), which leads to, e.g., conspicuously high Hf_N/Zr_N (3–9). This characteristic is not present in the marginal series gabbronorite.

Reef-type PGE-enriched zone

The highest concentration of PGEs in the Näränkävaara layered series is found along the border zone between the ultramafic and the mafic units, at a stratigraphic height of about 2350–2400 m (highlighted in Fig. 5). This PGE-enriched zone is intersected by four drill holes (MUV-6, −16, −19, −22) and has a continuous strike of at least 5 km (Fig. 2). Intersections through the zone range from 20 to 85 m in thickness (typically 25 m), with continuous anomalous 2PGE + Au

concentrations in the 50–500 ppb range (Fig. 9). Even though this PGE-enriched zone may not merit the term PGE reef, we refer to it as the *Salmilammit reef* (SL reef) coined after the location of discovery.

Petrography of the Salmilammit reef (SL reef)

The SL reef is hosted in the unit PX-2, which exhibits a series of transitional mineral assemblages and textures between the serpentinized olivine-rich cumulates of unit PER-2 below, and the gabbronoritic units above. The PGE enrichment is typically confined to the upper half of the unit PX-2, beginning 10–20 m after the disappearance of olivine (i.e., end of unit PER-2, see Fig. 9). The footwall rocks are composed of medium-grained, equigranular olivine websterite and plagioclase websterite. These contain approximately 25 vol% of sparse but coarse subspherical poikilitic augite up to 2 cm in diameter, with intercumulus plagioclase increasing to 5–15 vol% after olivine disappears (Fig. 3b). The texture of the mineralized plagioclase websterite is distinct from the pyroxenitic unit below, marked by an increase in the amount of intercumulus augite to approximately 40 vol%, associated with general fining of grain size (Fig. 3c). Fine-medium-grained tabular orthopyroxene grains define lamination in some samples, with rare needle-like grains up to 3 cm long. Biotite appears in trace amounts, and minor quartz is found in drill hole MUV-16. Intercumulus plagioclase increases towards the top of unit to 10–30 vol%. Melagabbronorite with cumulus plagioclase and minor anorthosite form the hanging wall.

In SL reef samples, Ca-poor pyroxene is enstatite (En_{80}, Fs_{17}, Wo_3), Ca-rich pyroxene is augite (En_{49}, Fs_9, Wo_{42}), and plagioclase is An_{60}. Mineral compositions in drill hole MUV-16 are slightly more evolved with approximately 10% lower An and 5% lower En. Two grains of apatite have been analyzed from drill hole MUV-19, both being chlorapatites with 4–6.5 wt% Cl.

The same sequence of cumulates is found in all examined drill holes, but the PGE enrichment is somewhat erratic in its distribution. In the easternmost drill hole (MUV-22) the PGE enrichment extends 2 m into the poikilitic augite containing subunit below (Fig. 9), which in the other intersections is

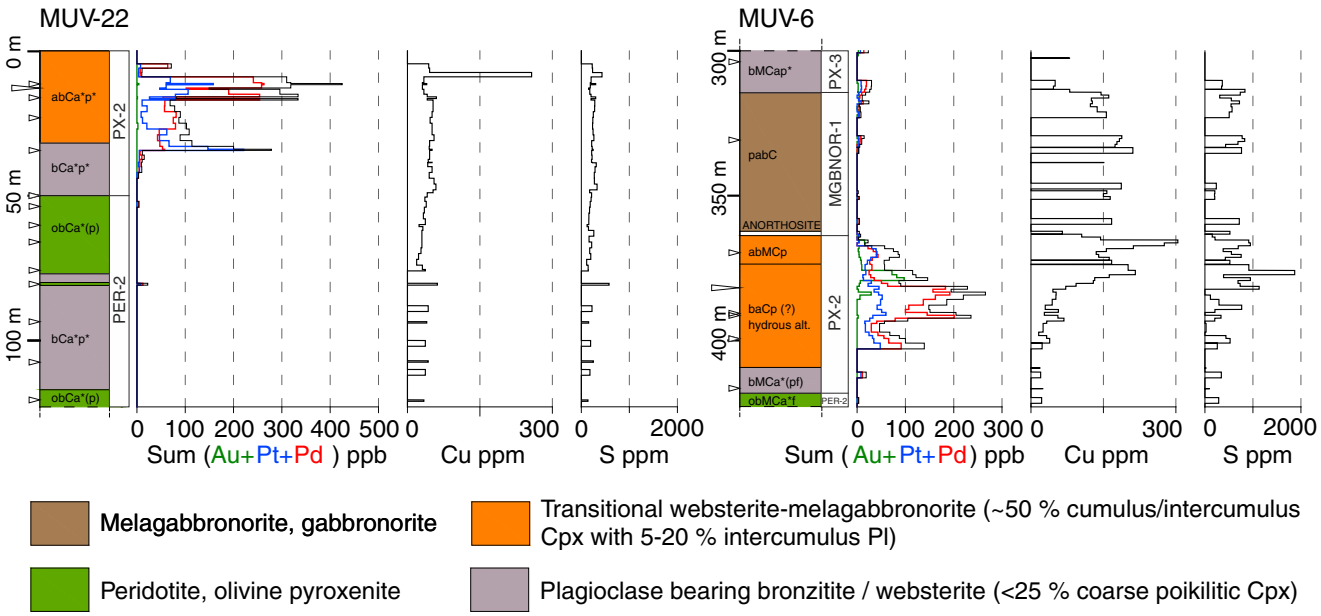

Fig. 9 Drill core intersections through the reef-type PGE-enriched zone (SL reef). Location of drill holes shown in Fig. 2. Columns on the left show lithology and correlation to units in Fig. 5, while plots on the right show whole-rock compositional variations (sum of Au + Pt + Pd plotted in black, Au in green, Pt in blue, Pd in red; Cu and S in black in separate plots). Small arrows show thin section locations, large arrows show combined thin section and mineral analysis (EPMA) locations. The same sequence of cumulus lithologies and textures is encountered in all four drill holes, with PGE-enrichment approximately 20 m after disappearance of olivine (i.e., above unit PER-2). MUV-6 exhibits a distinct Pd-peak followed by a Cu-peak, typical for an offset-type PGE-reef (Mungall 2007). Cumulus terminology after Irvine (1982) with the exception that intercumulus phases are listed as suffix with poikilitic phases denoted with an asterix

barren of PGEs. In the westernmost drill hole (MUV-16), the enrichment extends about 10 m into the first melagabbronorites of the mafic zone reaching a total thickness of 85 m.

Another PGE enrichment is found in the unit PX-1B, about 150 m below the SL reef. This lower PGE-enriched zone is about 5–20 m thick, and is hosted in plagioclase-bearing pyroxenite, 30 m below the lower contact of unit PER-2 (intersected by MUV-1 and MUV-3 in Fig. 4). Only three assays are available from this intersection, with grades of 100–250 ppb 2PGE + Au (~2150 m in Fig. 5). The host whole-rock compositions are slightly more primitive compared to the SL reef.

Chalcophile element geochemistry

Chalcophile element concentrations of SL reef samples are presented in Table 3. Intersections through the SL reef have an approximately 10 m thick Pd-rich peak with an average of 200–300 ppb Pd (highest 423 ppb) with Pd values tailing off to background values above and below (Fig. 9). The PGE enrichment is clearly Pd-dominated, with the Pd/Pt ratio varying between 0.5–8 (average 2.9). Normalized to 100 wt% sulfide, Pd contents varies between 50 and 300 ppm (Table 3). In drill hole MUV-22, the PGE enrichment begins in the poikilitic augite subunit below the typical host rock with a thin 200 ppb Pt-peak offset about 10 m below the Pd-peak found in other sections (Fig. 9); this is the highest Pt concentration found in the SL reef. Au contents are low with an average of 15 ppb.

Highest base metal and S concentrations are typically offset above the Pd-peak (see MUV-6 in Fig. 9). Even though the PGE enrichment is associated with base metal sulfides, the PGE-enriched samples are low on sulfur with 480 ppm S on average. Highest S in a PGE-enriched sample is 1870 ppm in drill hole MUV-6 (Fig. 9). The eastern drill holes MUV-19 and MUV-22 are very S-poor with an average 250 ppm (Fig. 9). Average Cu is 105 ppm (highest 262 ppm) and average Ni is 370 ppm (highest 573 ppm), with Ni/Cu ranging between 2 and 14 (3.2 on average). The stratigraphically lower PGE enrichment in the unit PX-1B (~2150 m in Fig. 5) has higher average Cu (300 ppm) and S (1300 ppm) compared to the SL reef.

The PM-normalized metal pattern of SL reef samples defines a bell-shaped curve typical for PGE-reefs in layered intrusions (Fig. 10). Ru, Ir, and Os (IPGE) are depleted in comparison to the Pd, Pt, and Rh (PPGE), with a distinct Pd-peak, and a slight negative Ru-anomaly. Pd/Ir ratios form two groups which range between 20–80 and 140–160, with an average of 99. Cu/Pd ratios in the ultramafic zone are generally below 5000–8000, in the SL reef between 100 and 500, and increase to 10,000–100,000 immediately above the reef (Fig. 5).

Sulfides and PGM

The SL reef is sulfide-poor with generally less than 0.5 vol% sulfides, but in small localized patches or layers sulfide proportions may reach 1 vol%. Sulfides consist of pyrrhotite intergrown with lesser chalcopyrite and pentlandite. These are found as small, usually less than 0.5 mm anhedral grains interstitial to silicates, typically in contact with plagioclase or augite (Fig. 11a). In the western drill holes (MUV-6 and MUV-16 in Fig. 2), the host pyroxenites and melagabbronorites are variably altered to chlorite and amphiboles, with sulfides partly altered to pyrite and disaggregated by secondary amphiboles. The eastern drill cores (MUV-19 and MUV-22) are unaltered.

In SEM scanning, platinum group minerals (PGM) were only found in drill hole MUV-19, appearing as distinct submicrometer scale grains on sulfide grain boundaries and within silicates (Fig. 11b). The largest PGM grain (5 μm) was found in a sulfide–silicate grain boundary. The PGM have been too small for reliable identification, but the most common phases appear to be composed of Pd and Pt sulfides and arsenides. Singular qualitative analyses also include PdGe (marathonite) and an unknown PdSnAuAsFe mineral. PGE contents of the associated sulfide grains have not been determined.

Discussion

Parental magma

Marginal series as indicator of parental magma composition

Estimation of the parental magma composition of the Näränkävaara layered series was undertaken for two reasons: to facilitate future studies on the petrogenetic relationship between the layered series and the basal dunite, and to better estimate the mineral potential of the layered series.

The melagabbronorite unit intersected in the contact of the Näränkävaara basal dunite and the layered series represents a marginal series, because it exhibits a fine-grained, non-cumulate, heterogeneous texture, with a gradual change into the homogeneous equigranular bronzitite of the layered series. Similar, poorly developed < 20 m thick marginal series are found in the 2.44 Ga Kemi, Tornio, and Penikat intrusions and in the Portimo complex (Fig. 1) (Iljina & Hanski 2005). An average composition of the layered series was calculated

Table 3 Chalcophile element concentrations from the Näränkävaara reef-type PGE-enriched zone (SL reef), with comparisons to other Finnish 2.45 Ga PGE reefs. Values in parentheses normalized to 100 wt% sulfide

Drill hole	Sample depth (m)	S ppm	Cu ppm (wt%)	Ni ppm (wt%)	Au ppb (ppm)	Pd ppb (ppm)	Pt ppb (ppm)	Ru ppb (ppm)	Rh ppb (ppm)	Ir ppb (ppm)	Os ppb (ppm)	Pd/Pt	Ni/Cu	Pd/Ir
MUV-6	381.5	600	30	430	8.0	203.0	62.0	3.0	6.0	3.0	1.0	3.3	14.3	68
			(2)	(25)	(5)	(117)	(36)	(1.7)	(3.5)	(1.7)	(0.6)			
MUV-16	56.7	600	160	310	29	362	118	2.0	5.0	2.0	< 1	3.1	1.9	181
			(9)	(18)	(17)	(211)	(69)	(1.2)	(2.9)	(1.2)				
MUV-16	61.0	300	80	270	14	305	93	< 1	6.0	2.0	1.0	3.3	3.4	153
			(9)	(30)	(15)	(334)	(102)		(6.6)	(2.2)	(1.1)			
MUV-19	7.55	400	70	470	6	423	41	3.0	3.0	3.0	2.0	10.3	6.7	141
			(6)	(37)	(5)	(337)	(33)	(2.4)	(2.4)	(2.4)	(1.6)			
MUV-22	11.3	300	40	480	4	263	158	3.0	5.0	3.0	1.0	1.7	12.0	88
			(4)	(48)	(4)	(264)	(158)	(3.0)	(5.0)	(3.0)	(1.0)			
MUV-22	15.9	300	60	380	1	54	26	2.0	8.0	3.0	1.0	2.1	6.3	18
			(6)	(40)	(1)	(56)	(27)	(2.1)	(8.4)	(3.1)	(1.0)			
Comparisons to PGE reefs in the Penikat intrusion														
AP[a]		4440	1350	830	350	7125	1965	19	210	42	20	3.6	0.61	170
			(11.1)	(6.9)		(588)	(162)							
SJ[b]		1300	600	1600	83	2700	2667	123	373	99	61	1.0	2.7	27
			(14.1)	(37.7)		(636)	(628)							
PV[c]		7900	2500	2400	270	2317	3913	108	92	77	54	0.6	1.0	30
			(11.4)	(10.9)		(105)	(178)							
Comparisons to PGE reefs in the Portimo complex														
SK[d]		4540	3600	800	340	9975	2848	47	330	65	32	3.5	0.2	153
			(27.5)	(6.1)		(763)	(217)							
RK[e]		2910	2490	630	210	7240	1630	24	171	32	28	4.4	0.25	226
			(29.3)	(7.4)		(851)	(191)							

[a] Ala-Penikka I reef, Halkoaho et al. (1990b); [b] Sompujärvi low-sulfide reef, Halkoaho et al. (1990a); [c] Paasivaara reef, Huhtelin et al. (1990); [d] Siika-Kämä reef, Iljina (1994); [e] Rytikangas reef, Iljina (1994). Recalculation of whole-rock compositions to 100% S after Barnes & Lightfoot (2005)

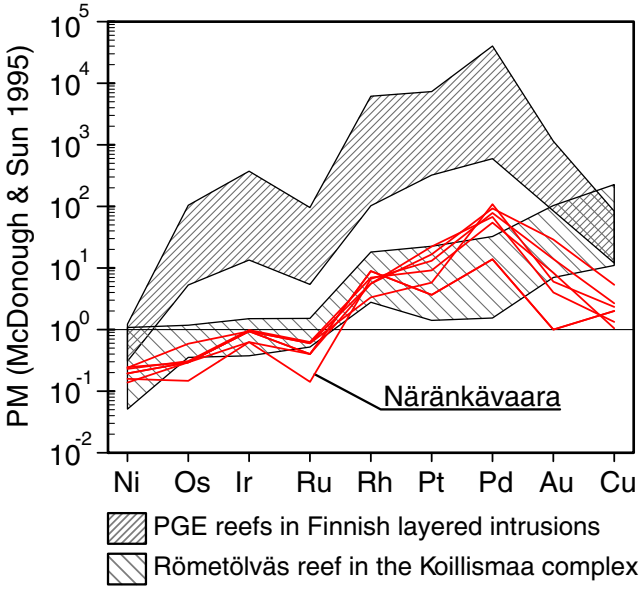

Fig. 10 Primitive mantle-normalized (McDonough & Sun 1995) metal patterns of whole-rock samples from the reef-type PGE-enriched zone in red (SL reef, samples listed in Table 3). Fields show comparisons to other Finnish 2.45 Ga PGE reefs in the Penikat intrusion (Sompujärvi, Ala-Penikka, and Paasivaara reefs), the Portimo complex (Siika-Kämä and Rytikangas reefs), and the Western Intrusions of the Koillismaa complex (Römetölväs reef; references in Table 3)

by weighting average unit compositions according to their stratigraphic heights (calculations in Appendix 3)—the basal dunite was excluded as discussed later. The weighted average composition was found to be quite similar to the marginal series composition (Table 2; plotted in Fig. 7). Both have high Ni and Cr contents relative to MgO compared to the typical gabbronorites of the layered series (Fig. 6).

To further test this marginal series parental magma hypothesis, we compared the observed crystallization sequences to the results of a fractional crystallization model performed with MELTS for the marginal series gabbronorite composition (rMELTS 1.2.0; Gualda et al. 2012; Ghiorso & Gualda 2015). In the model, the system was assumed to be dry and FeO/FeO^{tot} was assumed to be 0.85 (average FeO/Fe_2O_3 from Alapieti 1982). Crystallization sequence, as inferred from the relationships of the cumulus phases in the layered series, proceeds in the order: *Ol→Opx→Cpx→Pl→Ilm→Mag→Qz*. The model results in the same crystallization sequence, with *Opx* preceding *Cpx*, when P is 1–4 kbar. Modeled mineral compositions fit measured mineral compositions (Alapieti 1982; Telenvuo 2017) best at P of 2 kbar (Fig. 6). In the 2 kbar model, the first olivine to crystallize is Fo_{91} at 1400 °C. Orthopyroxene joins the liquidus at 1300 °C after 12 wt% fractionation of olivine. The most primitive olivine suggested by the MELTS model (Fo_{91}) has not been found in the analyzed cumulate rocks of the layered series. This may be due to (1) bias in sampling or mineral analyses, or (2) primitive olivine having accumulated elsewhere (e.g., deposits similar to the basal dunite, as discussed later). At the modeled *Ol–Opx* boundary, however, the modeled mineral compositions ($Fo_{87.5}$ and En_{86}) are very close to the compositions measured from the base of unit PER-1 ($En_{87.5}$ and $En_{85.3}$; Telenvuo 2017). The modeled temperature for the *Opx–Cpx* transition (~ 1230 °C) is also similar to that modeled with two-pyroxene thermometry (1200–1100 °C; Alapieti 1982).

As shown in the inset in Fig. 7a, the average olivine composition extrapolated to the Mg-Fe join from the PER-1 and PX-1 cumulates is approximately Fo_{87}. The ultramafic cumulates of units PER-1 and PX-1 can be modeled as mixtures of approximately Fo_{87} olivine, orthopyroxene ± clinopyroxene, and a liquid corresponding to the marginal series composition (Fig. 6 and 7a), although the actual interstitial liquid is likely to be more evolved.

In summary, the MELTS modeling results and the similarity of the marginal series gabbronorite to the weighted average

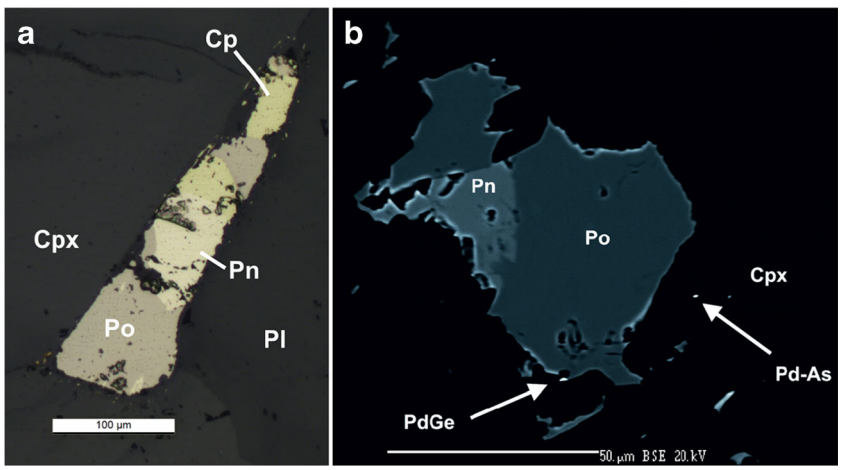

Fig. 11 **a** Primary magmatic sulfide bleb interstitial to clinopyroxene and plagioclase (sample *MUV-22 11.45m*; reflected light; scale bar 100 µm). **b** SEM image of intergrown pyrrhotite-pentlandite grain with a ~ 1 µm PdGe grain on the sulfide-silicate grain boundary; a similar sized PdAs grain is enclosed in augite (sample *MUV-19 7.85m*; scale bar 50 µm)

composition suggest that the marginal series represents a reasonable approximation of the parental magma composition of the Näränkävaara layered series.

Geochemical characteristics of the parental magma

Within the Fennoscandian shield, the parental magmas of the 2.5–2.4 Ga layered intrusions have been interpreted as siliceous high-Mg basalts, sourced from the asthenospheric mantle, with the magmas having incorporated substantial amounts of felsic continental crust during ascent (Amelin & Semenov 1996; Puchtel et al. 1997; Hanski et al. 2001; Yang et al. 2016; Maier et al. 2018). A crustal contamination signature is evident in the intrusions as LREE-enrichment with La_N/Yb_N of 3–10; and in fractionated PM-normalized trace element patterns, variably enriched in LILE, Th, and U, with prominent negative Nb, Ta, Ti, and P anomalies (Iljina & Hanski 2005; Vuollo & Huhma 2005; Maier et al. 2018).

The parental magma of the Näränkävaara layered series displays all the characteristics of a crustal signature described above (Fig. 8a–b), with slightly more pronounced enrichment in LILE, Th and U compared to other Finnish ~2.45 Ga layered intrusions and dykes. Similar levels of enrichment are found in the komatiitic basalts of the Vetreny belt and in the Bushveld B1 magma, both of which show signs of contamination by up to 15–20 wt% of crustal or sub-continental lithospheric mantle (SCLM) material (Puchtel et al. 1997; Barnes et al. 2010; Kulikov et al. 2010; Günther et al. 2018). The Näränkävaara parental magma also displays a notable positive Sr anomaly with 200–600 ppm Sr (Fig. 8b), similar to average concentrations of Sr in continental crust (300 ppm; Rudnick & Fountain 1995).

Major element concentrations in the Näränkävaara parental magma also point to a relatively high degree of contamination with felsic materials. Its primitive characteristics—high MgO (14–15 wt%), Ni (300–500 ppm), and Cr (1450–1750 ppm)—are concurrent with untypically high SiO_2 (54–55 wt%) compared to the other Finnish layered intrusions (Alapieti & Lahtinen 2002; Iljina & Hanski 2005). The Vetreny belt komatiitic basalts are described as having high MgO of 9–18 wt%, but contain < 53 wt% SiO_2 (Kulikov et al. 2010). A group of fractionated ~2.45 Ga boninite-norite dykes with MgO between 3 and 20 wt% (Vuollo & Huhma 2005) covers the compositional range of the inferred parental magmas of the Finnish layered intrusions. The Näränkävaara parental magma plots in the outer limit of the compositional field of these dykes in regard to the concurrently high SiO_2, MgO, and Cr.

Implications of the marginal series for the basal dunite

If the Näränkävaara layered intrusion magma developed a marginal series against the basal dunite, then the basal dunite must predate the emplacement of the layered series (2436 ± 5 Ma; Alapieti 1982) and thus belong to an earlier magmatic event. The petrogenesis of the Näränkävaara basal dunite has not been studied in detail, however, and the absolute age difference is not known. Taking into account the sheared contact between the basal dunite and the layered series, and the ubiquitous faulting present in the intrusion—with dislocations up to several hundred meters—it is conceivable that the marginal series was originally emplaced against a roof wall of Archean basement, and later faulted into its current position.

The Näränkävaara basal dunite is distinctly more extensive, magnesian, and homogeneous in composition compared to other dunitic or peridotitic units in ~2.45 Ga Finnish intrusions. Dunitic cumulates can be formed by accumulation of olivine in basal sections of (rhythmic) mafic intrusions, but continuous, up to 2 km thick dunites in layered intrusions are rare. The mafic-ultramafic Burakovsky intrusion in Russian Karelia (Fig. 1) hosts an up to 3- to 6-km-thick relatively homogeneous basal dunite (Chistyakov & Sharkov 2008), but the exact method of its formation has not been worked out. Dunitic cumulates up to 1 km thick are present in the Great Dyke of Zimbabwe, where they are found interlayered with chromitite seams and minor harzburgites, having formed over several magma pulses (Wilson 1996). Formation of an extensive olivine adcumulate from a parental magma with 14–15 wt% MgO would likely require repeated recharge or flow-through. If the Näränkävaara basal dunite belongs to the same ~2.45 Ga magmatic event as the layered series, then it would probably represent an open system feeder channel similar to the Great Dyke, having fed volcanic systems such as the 2.44 Ga komatiitic basalts described from the Vetreny belt (Kulikov et al. 2010).

Thick dunite successions may also represent Archean komatiitic environments such as portions of lava flow channels (Barnes et al. 1988). Therefore, another possibility is that the basal dunite represents an older, Archean komatiitic wall rock to the layered intrusion, a segment of a greenstone belt that are common in the Archean of the Fennoscandian shield. The petrogenesis of the basal dunite is beyond the scope of this article and will be assessed in future studies.

Magmatic evolution of the layered series

The general magmatic evolution of the Näränkävaara layered series has been inferred from variations in cumulate whole-rock compositions (e.g., Figs. 5 and 7). These give the impression of mostly closed system fractionation of a large initial batch of magma, interrupted by open system recharge: first

before the onset of plagioclase fractionation (i.e., the PER-2 reversal and the melagabbronorite subzone); and later in the gabbronorites of the mafic zone (i.e., the PER-3 reversal). The Fe-enrichment in the gabbronorites caused by late crystallization of magnetite indicates a tholeiitic fractionation trend (Fig. 7).

Petrography indicates that crystallization in the ultramafic and melagabbronoritic zones is controlled by cumulus processes. The sharply increasing Zr contents to about 100–200 ppm provide strong evidence that the gabbronorites from unit GBNOR-1 upwards represent orthocumulate or melt compositions (Fig. 5). MELTS modeling of the parental magma shows that plagioclase begins to crystallize after about 50% fractionation. Assuming Zr was completely incompatible, this would correspond to doubling of the Zr in the parental magma to 80–120 ppm in the residual melt (cf. marginal series composition in Table 2). This suggests a near-liquid composition for the gabbronorites, although cumulus plagioclase is observed in drill core throughout the unit.

Some of the more evolved gabbronoritic rocks are untypically biotite- and alkali-rich (Figs. 5 and 7b). No xenoliths or other direct evidence of in-situ wall-rock assimilation has been found, so any possible assimilant has completely mixed with the magma (whether before or after emplacement), with the incompatible elements enriched in the residual melt from which the gabbronorites crystallized.

Evidence for magma replenishment

Two abrupt reversals restart differentiation from more primitive compositions (units PER-2 and PER-3 in Figs. 7a–b). The reversals are interpreted as new pulses of relatively primitive magma into a partly differentiated and consolidated magma chamber. This is supported by the reappearance of cumulus olivine after a series of lower temperature cumulates, and increase in MgO, Ni, and Cr in whole-rock compositions (Figs. 5 and 6). Chromitite seams are not found anywhere in the layered series, the formation of which could be expected at the lower contacts of the peridotitic reversals (Irvine 1975). At the base of unit PER-2, orthopyroxene En-contents increases by 1–2 mol% compared to the unit below (Telenvuo 2017). This increase is similar in scale as in the rhythmic reversals in the pyroxenite successions of the Great Dyke, attributed to influxes of primitive magma (Wilson 1996).

A weakly PGE-enriched tail following the PER-3 reversal (~ 50 ppb 2PGE + Au; Fig. 5) suggests influx of new comparatively PGE-rich magma. The Fe-Ti-oxide-bearing gabbronorites immediately below PER-3 are geochemically similar to those found at the gabbronorite-diorite contact (Fig. 5). Modeling indicates Fe-Ti oxide and sulfide saturation occur after about 70–80% fractional crystallization of the parental magma, suggesting that differentiation of the residual magma may have advanced quite far at the time of the PER-3 reversal. The alteration textures and high modal biotite found in the PER-3 peridotites and pyroxenites are likely related to mixing of the incipient PER-3 magma with the volatile and incompatible element enriched residual magma.

Petrographical and compositional similarities (e.g., trace element ratios) between the three peridotitic units point to a single parental magma type. They all contain high Cr, so none of them represent the low-Cr magma type described from the mafic and megacyclic layered intrusions of the Tornio-Näränkävaara belt (Iljina & Hanski 2005). For PER-1 and PER-2, there is a strong positive correlation between whole-rock (and olivine) MgO and Ni (Fig. 6), implying a shared parental magma with its composition controlled by olivine fractionation. The decreasing olivine Fo contents between the reversals suggests progressive fractionation in a parallel staging magma chamber before emplacement in the layered series (similar to Penikat intrusion, Maier et al. 2018). The gradual increase in incompatible elements with stratigraphic height from PER-1 to PER-2 to PER-3 (Fig. 6) is at least partially explained by increasing intercumulus material. This may also, at least in part, explain the decrease in Fo content between the reversals, because increase in modal intercumulus facilitates post-cumulus re-equilibration of olivine to a lower Fo content (the ”trapped liquid shift”; Barnes 1986). The higher Ni-content in the PER-3 olivine at a lower Fo content compared to PER-2 suggests a less fractionated source for PER-3.

Transition zone between ultramafic and mafic zones

The transition zone from the ultramafic to the mafic zone (melagabbronorite subzone) includes several smaller alternating reversals between pyroxenite and melagabbronorite (note Ni between units PER-2 and GBNOR-1 in Fig. 5; also smaller reversals in Fig. 7b). Whole-rock compositions of the alternating units evolve towards a lower Mg# upwards in stratigraphy, with the compositional changes getting progressively smaller, until reaching the homogeneous unit GBNOR-1. The origin of these compositional oscillations is not known. It can be speculated that at least the unit PX-3 is related to magmatic replenishment, based on the slight PGE enrichment associated with it (Fig. 5). It is possible that the melagabbronorite subzone represents a series of small replenishments of primivite magma, followed each time by fractionation and deposition of a relatively primitive basal cumulate unit (high-Ni units in

Fig. 5), followed by consequent convective overturn (mixing) and deposition of a more evolved cumulate layer (Huppert & Sparks 1984).

The chemical composition of the lowermost melagabbronorite unit (MGBNOR-1A) is distinct, with the lowest FeO/Al_2O_3 ratios (0.2–0.3) relative to Mg# (75–80) in the layered series. Outcrop samples from the SE block of the layered series (Heinivaara gabbronorites in Fig. 2) fall into the same limited compositional range, some with anomalous 2PGE + Au of 100–200 ppb. These outcrops very likely represent the stratigraphic level of the transition zone in the SE block.

SL reef

Classification, characteristics, and comparisons

The uneconomic PGE enrichment in the Näränkävaara layered series (SL reef) can be classified as a stratabound sulfide-associated PGE-mineralization, i.e. reef type. The SL reef can also be classified as an offset-reef, because the highest Cu, S, and Au concentrations are offset about 10 m above peak PGE concentrations (Fig. 9) (Mungall 2007). High-grade offset-type PGE reefs in a similar stratigraphic position are found in, e.g., the Great Dyke (Lower and Main Sulfide Zones; Wilson 1996, 2001) and the Munni Munni complex (Ferguson reef; Hoatson & Keays 1989; Barnes & Hoatson 1994). The low-grade SL reef is similarly found in a relatively thick and homogeneous cumulate unit towards the top of the ultramafic zone, 5–20 m below the first appearance of cumulus plagioclase. For some reason, the processes that produced high-grade mineralization in the other two intrusions did not occur in Näränkävaara.

PGE reefs in a similar stratigraphic position as the Näränkävaara SL reef have not been described from other 2.44 Ga mafic-ultramafic layered intrusions of the Tornio-Näränkävaara belt. The Sompujärvi (SJ), Paasivaara (PV) and Ala-Penikka (AP) reefs of the Penikat intrusion, and the Siika-Kämä (SK) and Rytikangas (RK) reefs of the Portimo complex (Fig. 1) are located in megacyclic intrusions (Alapieti & Lahtinen 2002; Iljina et al. 2015 and references therein). The stratigraphically lowermost PGE reefs are found near the bases of megacyclic units (SJ, SK) at a level where the high-Cr megacyclic units transition into low-Cr units. In addition, reefs are found within the megacyclic units in variable gabbroic and anorthositic units from this stratigraphic position upwards (AP, PV, RK) (Iljina et al. 2015). As described previously, the Näränkävaara SL reef apparently does not occur at a level where there was influx of a Cr-poor magma. In the Western Intrusions of the KLIC, the low-grade Römetölväs (RT) reef is associated with an influx of primitive magma into evolved gabbroic cumulates (Karinen 2010).

Sulfide tenors and metal ratios in the SL reef samples attest of a high R-factor PGE reef forming event. Large inaccuracies are introduced when compositions with less than 2–3 wt% sulfide are normalized to 100 wt% sulfide (Barnes & Lightfoot 2005). The SL reef is sulfide-poor, and the calculations regarding sulfide tenor and R-factor are provided only to estimate their order of magnitude. The high PGE tenors found in the SL reef sulfides (50–300 ppm Pd normalized to 100 wt% sulfide) are slightly lower—but in a similar range—as those described from other sulfide associated PGE reefs in 2.45 Ga Finnish layered intrusions (see Table 3). The SL reef sulfide tenors correspond to R-factors (Campbell & Naldrett 1979) in the 10^5 range using marginal series from Table 2 as the original composition, and a Pd $D_{sil/sulf}$ of 10^5 (Mungall & Brenan 2014). Primitive mantle normalized metal patterns in Fig. 10 are also similar in shape between the SL reef and other sulfide associated PGE reefs from Finnish 2.45 Ga layered intrusions, except for the lower amounts of PGE in Näränkävaara.

Recalculating the 2PGE + Au grades of the on average 25 m thick SL reef to a vertical thickness of 1 m corresponds to concentrations of 2.5–4.5 ppm 2PGE + Au, depending on cutoff. By comparison, the Merensky reef is approximately 1 m thick with an average of 5 ppm of 2PGE + Au (Bristow et al. 1993). This implies at least a moderate PGE budget in the SL reef-forming magma; however, the concentrations have been diluted over a large vertical extent. On the Cu/Pd vs. Pd diagram in Fig. 12, samples from the SL reef plot on a similar trend as other Finnish PGE reefs (except RT) that indicates high R-factors in the 10^5 range (Barnes et al. 1993). However, the highest Pd concentrations in the SL reef (~ 0.5 ppm Pd) are much lower in comparison to those of the other Finnish PGE reefs (5–10 ppm Pd). According to the model, this is a function of the other reefs having formed more sulfides in the 1 vol% range, compared with the < 0.1 vol% of SL reef. This suggests that the SL reef sulfides were formed from a relatively PGE-fertile magma under high-R factor conditions, but that the low amount of precipitated and accumulated sulfides at the time of reef forming may have been a limiting factor for the formation of a high-grade PGE reef.

Sulfur saturation and hypothesis for origin of SL reef

The SL reef sulflides and PGM exhibit textures commonly found in primary magmatic sulfides formed through cooling and fractionation of sulfide solid solutions (Barnes & Lightfoot 2005). It is possible that some post-cumulus remobilization of sulfides and PGEs has occurred (drill holes MUV-6 and MUV-16), but it is thought to be minor on the scale of the whole layered series, and not a primary mechanism for the formation of the PGE-enrichment.

Significant changes in the Cu/Pd ratio through the magmatic stratigraphy of a layered intrusion can indicate sulfide saturation and reef-forming events (Barnes et al. 1993). The Cu/Pd ratios of the marginal series (~8000) and the weighted average of the layered series (~5000) are below primitive mantle ratios (8000–10,000), implying a PGE-fertile melt (Barnes & Lightfoot 2005). The Cu/Pd ratios in the ultramafic zone also generally remain below 5000–8000 (Fig. 5), suggesting that significant sulfide saturation has not occurred below the SL reef level. The SL reef is associated with a major change in Cu/Pd, from < 5000 to 30,000–50,000 (highest 200,000) in the melagabbronorites above the reef. This suggests that formation of the SL reef was the first major sulfide saturation event in the layered series magma. Rocks of the mafic zone above the SL reef are commonly sulfide-bearing with about 500 ppm S but are almost barren of PGEs (Fig. 5). This suggests that formation of the SL reef depleted the residual magma of PGEs.

The offset-type metal distribution in the SL reef and high sulfide tenor and R-factor suggest that after precipitation the sulfides equilibrated in contact with a large body of (convecting) magma with the PGEs concentrated into the first formed sulfides by the higher distribution coefficients (Barnes 1993; Wilson 2001) and higher rates of diffusion (Mungall 2002) of the PGEs compared to base metals. The first sulfides would thus deplete the remaining magma of PGEs. The offset-distribution also suggests that the sulfides were accumulated and disconnected from the melt-interface relatively quickly, thus prohibiting further equilibration. The same argument would also imply only minor redistribution of sulfides after precipitation, as this would be assumed to homogenize the metal distribution. Rather, these observations point to continuous in-situ formation of sulfides in contact with a convecting magma (see Latypov et al. 2015).

Excluding samples with > 20 ppb Pd, the peridotites and pyroxenites below PER-2 have a combined average Cu/Pd ratio of approximately 5000, whereas from PER-2 upward peridotitic and pyroxenitic samples have a higher average of approximately 10,000 (Fig. 12). This implies that the magma associated with the PER-2 reversal may have already been PGE-depleted by the time of its emplacement in the layered series, relative to the original parental magma. Whether this had some impact on the low grade of the SL reef is not known.

It seems that PGE enrichment similar to the SL reef began to develop already about 50 m below the PER-2 reversal near the top of the unit PX-1B, and was probably halted by the PER-2 reversal (Fig. 5). This lower PGE enrichment is associated with similar changes in Cu/Pd ratios as the SL reef (Fig. 12). Perhaps the PER-2 magma was denser compared to the residual magma in the chamber, and, instead of causing turbulent pluming and mixing upon emplacement (like in Munni Munni; Barnes & Hoatson 1994), it spread out along the base of the chamber (like hypothesized for the Merensky Reef; Latypov et al. 2015). The high FeO and low SiO_2 contents would have inhibited sulfide saturation, possibly leading to reabsorption of existing sulfides. After deposition of olivine and pyroxene cumulates, the magma would have again reached S-saturation, possibly related to a FeO minima on the liquid line of descent caused by fractionation of mafic silicates (see Li & Ripley 2005). During the SL reef formation, silicates and a relatively small amount of sulfides fractionated continuously and simultaneously and both were accumulated more or less in-situ leading to the silicates "diluting" and extending the reef (Fig. 9). The first precipitated sulfides

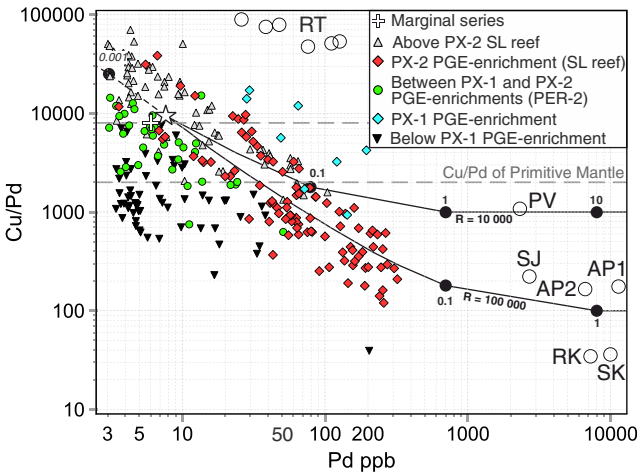

Fig. 12 Whole-rock compositions plotted on a Cu/Pd vs. Pd diagram. Star and model lines from Barnes et al. (1993): star indicates starting composition (7.6 ppb Pd, 80 ppm Cu); model lines show composition of sulfides in equilibrium with the starting composition at different R-factors; filled circles indicate compositions of rocks containing 0.1, 1, and 10 vol% of said sulfides. The steep downwards trend in SL reef samples indicates a R-factor of 10^5 similar to other 2.45 Ga Finnish PGE reefs (open circles). Excluding Pd-rich samples, samples from the PER-2 reversal upwards have, on average, higher Cu/Pd ratios than samples below. Abbreviations for PGE reefs in the Penikat intrusion: *SJ* Sompujärvi, *AP1-2* Ala-Penikka 1 and 2, *PV* Paasivaara; for the Portimo complex: *SK* Siika-Kämä, *RK* Rytikangas; and from the Koillismaa complex *RT* Römetölväs (references in Table 3)

efficiently scavenged the magma of PGEs and formed the offset-type metal distribution. The magma continued to crystallize at sulfide saturation almost throughout the mafic zone, with a slight recharge of PGEs brought in by the PER-3 magma (Fig. 5). Terminal sulfide saturation, barren of PGEs, was reached at the gabbronorite-diorite contact, probably brought on by a decrease in FeO related to Fe-Ti oxide fractionation.

Conclusions

Our data and observations lead to the following conclusions:

- The 2.44 Ga Näränkävaara layered intrusion represents a mafic-ultramafic layered series with a thick peridotitic-to-pyroxenitic ultramafic zone, and a gabbronoritic-to-dioritic mafic zone. The cumulates are relatively unaltered, and follow a tholeiitic fractionation trend with two reversals back to Mg-rich compositions. The reversals are thought to be caused by replenishment with magmas of broadly similar composition as the original parental magma of the layered series, but in different states of fractionation.
- Below the layered series is an extensive, approximately 2-km-thick basal dunite mostly composed of serpentinized olivine ad- and mesocumulates. The layered series includes a marginal series emplaced against the basal dunite, indicating that the basal dunite is older than the layered intrusion. By how much is not known.
- Layered series parental magma composition has been inferred from a marginal series melagabbronorite. It contains 54.6% SiO_2, 0.4% TiO_2, 11.0% Al_2O_3, 14.1% MgO, 8.6% FeO, 500 ppm Ni, 1750 ppm Cr, 6.1 ppb Pd, and 8.2 ppb Pt. The similarity of major and trace element concentrations between the Näränkävaara parental magma and other intrusions of the 2.44 Ga Tornio-Näränkävaara belt indicate that they belong to the same large scale magmatic event. The Näränkävaara parental magma represents a relatively primitive but highly contaminated end-member in the context of the early Paleoproterozoic Fennoscandian SHMB magmatism.
- The layered series hosts an uneconomic offset-type PGE reef (SL reef) along the mafic-ultramafic transition zone, in a similar stratigraphic location as in the Munni Munni and the Great Dyke intrusions. Metal ratios and sulfide tenors give evidence of a high R-factor PGE reef forming event, similar to those interpreted for other sulfide associated PGE reefs in 2.45 Ga Finnish layered intrusions.
- Low whole-rock PGE grades of the SL reef seem to be caused by low rate of sulfide accumulation relative to simultaneous silicate accumulation, leading to dilution of high-grade sulfides over an average thickness of 25 m. Influx of new, possibly PGE-depleted magma at the onset of sulfide saturation may have halted the reef-forming process and diluted the residual magma in regard to PGE.

Acknowledgements We would like to thank the reviewers Shenghong Yang and Stephen J. Barnes for valuable comments that greatly improved the manuscript and guest editor Ferenc Molnár for editorial handling of the manuscript. We would also like to thank the K.H. Renlund Foundation for providing a Ph.D. research grant to V. Järvinen. This work was also supported by Academy of Finland Grants 295129 and 306962 (J. Heinonen). The GTK projects linked to Ni-Cu-Co-PGE potential in Finland are thanked for providing the historical data and new analyses required for completion of this study. Lassi Pakkanen and Bo Johanson from GTK mineral laboratory are thanked for mineralogical analyses and guidance. Marko Moilanen and Leena Palmu from the University of Oulu are thanked for their help with historical XRF analyses. Pentti Järvinen is thanked for reviews of early versions of this manuscript. Special thanks to everyone involved with the GTK–University of Helsinki Eastern Lapland Komatiite project for establishing a fun, energetic, and highly motivated research team.

Funding information Open access funding provided by University of Helsinki including Helsinki University Central Hospital.

References

Akkerman JH (2008) Mineral exploration report Koillismaa-Naranka project (2005–2007) Akkerman Exploration B.V. and Nortec Ventures Inc joint venture. Geol Surv Finl, Hakku-database, Exploration report, 42 pp

Alapieti T (1982) The Koillismaa layered igneous complex, Finland—its structure, mineralogy and geochemistry, with emphasis on the distribution of chromium. Geol Surv Finl, Bulletin 319, 116 pp

Alapieti T, Lahtinen J (2002) Platinum-group element mineralization in layered intrusions of Northern Finland and the Kola Peninsula, Russia. In: Cabri LJ (ed) The geology, geochemistry, mineralogy and mineral beneficiation of platinum-group elements. CIM Special Volume 54, pp 507–546

Alapieti T, Hugg R, Piirainen T et al (1979) The ultramafic and mafic intrusion at Näränkävaara, northeastern Finland. Geol Surv Finl, Report of Investigation 35, 31 pp

Alapieti T, Filén BA, Lahtinen J et al (1990) Early Proterozoic layered intrusions in the northeastern part of the Fennoscandian Shield. Mineral Petrol 42(1–4):1–22. https://doi.org/10.1007/BF01162681

Amelin YV, Semenov VS (1996) Nd and Sr isotopic geochemistry of mafic layered intrusions in the eastern Baltic shield: implications for the evolution of Paleoproterozoic continental mafic magmas. Contrib Mineral Petrol 124(3–4):255–272. https://doi.org/10.1007/s004100050190

Amelin YV, Heaman LM, Semenov VS (1995) U-Pb geochronology of layered mafic intrusions in the eastern Baltic Shield: implications for the timing and duration of Paleoproterozoic continental rifting. Precambrian Res 75(1–2):31–46. https://doi.org/10.1016/0301-9268(95)00015-W

Auranen O (1969) Näränkävaaran ultraemäksinen massiivi. MSc thesis, University of Oulu (55 pp)

Barnes SJ (1986) The effect of trapped liquid crystallization on cumulus mineral compositions in layered intrusions. Contrib Mineral Petrol 93(4):524–531. https://doi.org/10.1007/BF00371722

Barnes SJ (1993) Partitioning of the platinum group elements and gold between silicate and sulphide magmas in the Munni Munni Complex, Western Australia. Geochim Cosmochim Acta 57(6): 1277–1290. https://doi.org/10.1016/0016-7037(93)90064-4

Barnes SJ, Hill RET (1995) Poikilitic chromite in komatiitic cumulates. Mineral Petrol 54(1–2):85–92. https://doi.org/10.1007/BF01162760

Barnes SJ, Hill RET, Gole MJ (1988) The Perseverance Ultramafic Complex, Western Australia: the product of a Komatiite Lava River. J Petrol 29(2):305–311. https://doi.org/10.1093/petrology/29.2.305

Barnes SJ, Hoatson DM (1994) The Munni Munni complex, Western Australia: stratigraphy, structure and petrogenesis. J Petrol 35(3): 715–751. https://doi.org/10.1093/petrology/35.3.715

Barnes S-J, Lightfoot P (2005) Formation of magmatic nickel sulfide ore deposits and processes affecting their copper and platinum group element contents. In: Hedenquist JW, Thompson JF, Goldfarb RJ (eds) Economic geology 100th anniversary volume. Society of Economic Geologist, pp 179–213. https://doi.org/10.1103/PhysRevE.70.021911

Barnes S-J, Couture JF, Sawyer EW et al (1993) Nickel-copper occurrences in the Belleterre-Angliers belt of the Pontiac Subprovince and the use of Cu-Pd ratios in interpreting platinum-group element distributions. Econ Geol 88(6):1402–1418. https://doi.org/10.2113/gsecongeo.88.6.1402

Barnes S-J, Maier WD, Curl EA (2010) Composition of the marginal rocks and sills of the Rustenburg Layered Suite, Bushveld Complex, South Africa: implications for the formation of the platinum-group element deposits. Econ Geol 105(8):1491–1511. https://doi.org/10.2113/econgeo.105.8.1491

Bayanova T, Ludden J, Mitrofanov FP (2009) Timing and duration of Palaeoproterozoic events producing ore-bearing layered intrusions of the Baltic Shield: Metallogenic, petrological and geodynamic implications. Geol Soc Lond Spec Publ 323:165–198. https://doi.org/10.1144/SP323.8

Bristow DG, Cawthorn RG, Harmer J et al (1993) Symposium on layering in igneous complexes, excursion guide. Aurora, 161 Mitchell Street, Pretoria West, 59 pp

Campbell IH, Naldrett AJ (1979) The influence of silicate:sulfide ratios on the geochemistry of magmatic sulfides. Econ Geo 74(6):1503–1506. https://doi.org/10.2113/gsecongeo.74.6.1503

Chistyakov AV, Sharkov EV (2008) Petrology of the early paleoproterozoic Burakovsky complex, southern Karelia. Petrology 16(1):63–86. https://doi.org/10.1007/s11495-008-1004-2

Elo S (1991) Geophysical indications of deep fractures in the Näränkävaara-Syote and Kandalaksha-Puolanka zones. In: Silvennoinen A (ed) deep fractures in the paanajärvi-kuusamo-koulajärvi area, Proceedings of a finnish-Soviet Symposium in finland on September 18–21, 1989. Geol Surv Finl, Spec paper 13:43–50

Ghiorso M, Gualda G (2015) An H2O–CO2 mixed fluid saturation model compatible with rhyolite-MELTS. Contrib Mineral Petrol 169(6):53. https://doi.org/10.1007/s00410-015-1141-8

Gualda GAR, Ghiorso MS, Lemons RV et al (2012) Rhyolite-MELTS: a modified calibration of MELTS optimized for silica-rich, fluid-bearing magmatic systems. J Petrol 53(5):875–890. https://doi.org/10.1093/petrology/egr080

Günther T, Haase K, Klemd R et al (2018) Mantle sources and magma evolution of the Rooiberg lavas, Bushveld Large Igneous Province, South Africa. Contrib Mineral Petrol 173(51):27–27. https://doi.org/10.1007/s00410-018-1477-y

Halkoaho T, Alapieti T, Lahtinen J (1990a) The Sompujärvi PGE reef in the Penikat layered intrusion, Northern Finland. Mineral Petrol 42(1–4):39–55. https://doi.org/10.1007/BF01162683

Halkoaho T, Alapieti T, Lahtinen J et al (1990b) The Ala-Penikka PGE reefs in the Penikat layered intrusion, Northern Finland. Mineral Petrol 42(1–4):23–38. https://doi.org/10.1007/BF01162682

Halkoaho T, Konnunaho J, Järvinen V et al (2017) A new reef-type PGE-enriched zone in the early Proterozoic Näränkävaara layered intrusion, north-eastern Finland. Proceedings of the 14th SGA Biennial Meeting, 20–23.8.2017, Quebéc

Halkoaho T, Konnunaho J, Niskanen M (2019) The Ni-(Cu-PGE) potential of Näränkävaara mafic-ultramafic complex. Geol Surv Finl, Hakku-Database, Open File Work Report, 22 pp

Hanski E, Walker RJ, Huhma H et al (2001) The Os and Nd isotopic systematics of c. 2.44 Ga Akanvaara and Koitelainen mafic layered intrusions in northern Finland. Precambrian Res 109(1–2):73–102. https://doi.org/10.1016/S0301-9268(01)00142-5

Hoatson DM, Keays RR (1989) Formation of platiniferous sulfide horizons by crystal fractionation and magma mixing in the Munni Munni layered intrusion, west Pilbara Block, Western Australia. Econ Geol 84(7):1775–1804. https://doi.org/10.2113/gsecongeo.84.7.1775

Hölttä P, Heilimo E, Huhma H et al (2012) Archaean complexes of the Karelia Province in Finland. In: Hölttä P (ed) The Archaean of the Karelia Province in Finland. Geol Surv Finl, Spec Paper 54:9–20

Huhma H, Cliff RA, Perttunen V et al (1990) Sm-Nd and Pb isotopic study of mafic rocks associated with early Proterozoic continental rifting: the Peräpohja schist belt in northern Finland. Contrib Mineral Petrol 104(3):369–379. https://doi.org/10.1007/BF00321491

Huhma H, Hanski E, Kontinen A et al (2018) Sm–Nd and U–Pb isotope geochemistry of the Palaeoproterozoic mafic magmatism in eastern and northern Finland. Geol Surv Finl, Bulletin 405, 150 pp

Huhtelin T (2015) The Kemi Chromite Deposit. In: Maier WD, Lahtinen R, O'Brien H (eds) Mineral deposits of Finland. Elsevier, Amsterdam, pp 165–178

Huhtelin T, Alapieti T, Lahtinen J (1990) The Paasivaara PGE reef in the Penikat layered intrusion, northern Finland. Mineral Petrol 42(1–4): 57–70. https://doi.org/10.1007/BF01162684

Huppert HE, Sparks RS (1984) Double-diffusive convection due to crystallization in magmas. Annu Rev Earth Pl Sc 12:11–37. https://doi.org/10.1146/annurev.ea.12.050184.000303

Iljina M (1994) The Portimo Layered Igneous Complex, with emphasis on diverse sulphide and platinum-group element deposits. PhD thesis, Acta Universitatis Ouluensis A258, University of Oulu, 158 pp

Iljina M (2003) Hanke 2106001. Pohjois-Suomen kerrosintruusiot 1996–2002 Loppuraportti. Geol Surv Finl, Hakku-Database, Report of project, 24 pp

Iljina M, Hanski E (2005) Layered mafic intrusions of the Tornio-Näränkävaara belt. In: Lehtinen M, Nurmi PA, Rämö OT (eds) Precambrian geology of Finland—key to the evolution of the Fennoscandian shield. Developments in Precambrian Geology, vol 14. Elsevier, Amsterdam, pp 101–137

Iljina M, Maier WD, Karinen T (2015) PGE-(Cu-Ni) deposits of the Tornio-Näränkävaara Belt of intrusions (Portimo, Penikat, and Koillismaa). In: Maier WD, Lahtinen J, O'Brien H (eds) Mineral deposits of Finland. Elsevier, Amsterdam, pp 134–164

Irvine TN (1975) Crystallization sequences in the muskox intrusion and other layered intrusions-II. Origin of chromitite layers and similar deposits of other magmatic ores. Geochim Cosmochim Acta 39: 991–1020. https://doi.org/10.1016/0016-7037(75)90043-5

Irvine TN (1982) Terminology for layered intrusions. J Petrol 23(2):127–162. https://doi.org/10.1093/petrology/23.2.127-a

Jensen LS (1976) A new cation plot for classifying subalkalic volcanic rocks. Ontario Division of Mines, miscellaneous paper 66, 22 pp

Karinen T (2010) The Koillismaa Intrusion, northeastern Finland—evidence for PGE reef forming processes in the layered series. Geol Surv Finl, Bulletin 404, 176 pp

Karinen T, Hanski E, Taipale A (2015) The Mustavaara Fe-Ti-V oxide deposit. In: Maier WD, Lahtinen J, O'Brien H (eds) Mineral deposits of Finland. Elsevier, Amsterdam, pp 179–194

Kulikov VS, Bychkova YV, Kulikova VV et al (2010) The Vetreny Poyas (Windy Belt) subprovince of southeastern Fennoscandia: an essential component of the ca. 2.5–2.4 Ga Sumían large igneous province. Precambrian Res 183(3):589–601. https://doi.org/10.1016/j.precamres.2010.07.011

Labtium Oy (2015). Sample preparation and analytical methods–Geochemistry, exploration and mining. https://www.labtium.fi/wp-content/uploads/2017/07/Labtium_Sample_preparation_and_analytical_methods.pdf

Lahtinen J (2005) Tutkimustyöselostus Näränkävaaran-Murtovaaran ultramafisella-mafisella kompleksilla valtauksilla Murtovaara 6, 8–19, 21–26, 32–34 vuosina 2001–2003 suoritetuista malmitutkimuksista. Geol Surv Finl, Hakku-Database, Exploration report, 9 pp

Latypov R, Chistyakova S, Page A et al (2015) Field Evidence for the In Situ Crystallization of the Merensky Reef. J Petrol 56(12):2341–2372. https://doi.org/10.1093/petrology/evg023

Le Bas MJ (2000) IUGS Reclassification of the High-Mg and Picritic Volcanic Rocks. J Petrol 41(10):1467–1470. https://doi.org/10.1093/petrology/41.10.1467

Lehtonen E, Heilimo E, Halkoaho T et al (2017) The temporal variation of Mesoarchaean volcanism in the Suomussalmi greenstone belt, Karelia Province, Eastern Finland. Int J Earth Sci 106(2):763–781. https://doi.org/10.1007/s00531-016-1327-y

Li C, Ripley E (2005) Empirical equations to predict the sulfur content of mafic magmas at sulfide saturation and applications to magmatic sulfide deposits. Mineral Deposita 40(2):218–230. https://doi.org/10.1007/s00126-005-0478-8

Maier WD, Halkoaho T, Huhma H et al (2018) The Penikat intrusion, Finland: geochemistry, geochronology, and origin of platinum–palladium reefs. J Petrol 59(5):967–1006. https://doi.org/10.1093/petrology/egy051

Makkonen HV, Halkoaho T, Konnunaho J et al (2017) Ni-(Cu-PGE) deposits in Finland—geology and exploration potential. Ore Geol Rev 90:667–696. https://doi.org/10.1016/j.oregeorev.2017.06.008

McDonough WF, Sun S-s (1995) The composition of the Earth. Chem Geol 120(3–4):223–253. https://doi.org/10.1016/0009-2541(94)00140-4

Mungall JE (2002) Kinetic controls on the partitioning of trace elements between silicate and sulphide liquids. J Petrol 43:749–768

Mungall JE (2007) Magmatic ore deposits. In: Holland HD, Turekian KK (eds) Treatise on geochemistry, vol 3. Elsevier, Amsterdam, pp 1–33

Mungall JE, Brenan JM (2014) Partitioning of platinum-group elements and Au between sulfide liquid and basalt and the origins of mantle-crust fractionation of the chalcophile elements. Geochim Cosmochim Acta 125:265–289. https://doi.org/10.1016/j.gca.2013.10.002

Mutanen T, Huhma H (2001) U-Pb geochronology of the Koitelainen, Akanvaara and Keivitsa layered intrusions and related rocks. In: Vaasjoki M (ed) Radiometric age determinations from Finnish Lapland and their bearing on the timing of Precambrian volcano-sedimentary sequences. Geol Surv Finl, Spec Paper 33:229–246

Nakamura N (1974) Determination of REE, Ba, Fe, Mg, Na and K in carbonaceous and ordinary chondrites. Geochim Cosmochim Acta 38(5):757–775. https://doi.org/10.1016/0016-7037(74)90149-5

Perttunen V, Vaasjoki M (2001) U-Pb geochronology of the Peräpohja schist belt, Northwestern Finland. In: Vaasjoki M (ed.) radiometric age determinations from Finnish Lapland and their bearing on the timing of Precambrian volcano-sedimentary sequence. Geol Surv Finl, Spec Paper 33:45–84

Piirainen T, Hugg R, Aario R et al (1978) Koillismaan malmikriittisten alueiden tutkimusprojektin loppuraportti 1976. Geol Surv Finl, Report of Investigation 18, 51 pp

Puchtel IS, Haase KM, Hofmann AW et al (1997) Petrology and geochemistry of crustally contaminated komatiitic basalts from the Vetreny Belt, southeastern Baltic Shield: evidence for an early Proterozoic mantle plume beneath rifted Archean continental lithosphere. Geochim Cosmochim Acta 61(6):1205–1222. https://doi.org/10.1016/S0016-7037(96)00410-3

Rudnick RL, Fountain DM (1995) Nature and composition of the continental crust: a lower crustal perspective. Rev Geophys 33(3):267–309. https://doi.org/10.1029/95RG01302

Salmirinne H, Iljina M (2003) Koillismaan kerrosintruusiokompleksin tulokanavamuodostuman painovoimatulkinta ja alueen malmimahdollisuudet (osa 1). Geol Surv Finl, Hakku-Database, Archival report, 23 pp

Telenvuo B (2017) Kumulusstratigrafia ja mineraalien kryptinen vaihtelu Kuusamon Näränkävaaran kerrosintruusion luoteisosassa. MSc thesis, University of Oulu, 83 pp

Tiira T, Janik T, Kozlovskaya E et al (2014) Crustal architecture of the Inverted Central Lapland rift along the HUKKA 2007 profile. Pure Appl Geophys 171(7):1129–1152. https://doi.org/10.1007/s00024-013-0725-3

Vesanto J (2003) Kaivoslain 19 §:n mukainen tutkimustyöelostus Kuusamon Näränkävaaran kerrosintruusion alueella valtauksilla Murtovaara 1–5, 7, 20, 30, 31, 36, 37, 41–71 suoritetuista malmitutkimuksista. Geol Surv Finl, Hakku-Database, Exploration report, 9 pp

Vuollo J, Huhma H (2005) Paleoproterozoic mafic dikes in NE finland. In: Lehtinen M, Nurmi PA, Rämö OT (eds) Precambrian geology of Finland—key to the evolution of the Fennoscandian shield.

Developments in Precambrian Geology, vol 14. Elsevier, Amsterdam, pp 195–236

Whitney DL, Evans BW (2010) Abbreviations for names of rock-forming minerals. Am Mineral 95(1):185–187. https://doi.org/10.2138/am.2010.3371

Wilson AH (1996) The great dyke of Zimbabwe. In: Cawthorn RG (ed) Layered intrusions. Developments in Petrology, vol 15. Elsevier, Amsterdam, pp 365–402

Wilson AH (2001) Compositional and Lithological Controls on the PGE-bearing Sulphide Zones in the Selukwe Subchamber, Great Dyke: a Combined Equilibrium–Rayleigh Fractionation Model. J Petrol 42(10):1845–1867. https://doi.org/10.1093/petrology/42.10.1845

Yang S, Hanski E, Li C et al (2016) Mantle source of the 2.44–2.50-Ga mantle plume-related magmatism in the Fennoscandian shield: evidence from Os, Nd, and Sr isotope compositions of the Monchepluton and Kemi intrusions. Mineral Deposita 51(8):1055–1073. https://doi.org/10.1007/s00126-016-0673-9